Interaction Notes

Note 635

2 February 2020

High-Power Electromagnetics (HPEM) Testing and Analysis of Swiss Civil Defense Facility Using an Impulse Radiating Antenna (IRA) in both Transient and CW Operation

F.M. Tesche
EMConsultant (Retired)

D. V. Giri
Pro-Tech, 324 Washington Street, # 202, Wellesley, MA 02481
Dept. of ECE, University of New Mexico, Albuquerque, NM 87131

and

P.F. Bertholet[#], A. Kaelin*, A. Jaquier and M. Nyffeler
armasuisse , Wissenschaft und Technologie
Fachbereich Kommunikation und elektromagnetischer Schutz
Feuerwerkerstrasse 39, 3602 Thun, Switzerland

([#] P. F. Bertholet is Retired from armasuisse)

(* Dr. Kaelin is currently with EMProtec GmbH, Hinwil, Switzerland)

Abstract

This note describes measurement results from a Swiss test-bed facility in Spiez, Switzerland, for responses to high-power electromagnetic (HPE) environments. The test data was gathered for both pulse and CW illuminations. The pulse illumination was accomplished by using the Swiss Impulse Radiating Antenna (Swiss IRA) system, fed by a commercial pulse generator. CW measurements were obtained using the same antenna and a network analyzer and wideband amplifier. This antenna and its characteristics are briefly discussed, and samples of the results of the measurements obtained in this test program are illustrated.

Contents

Abstract ii

Contents iii

Figures iv

Tables vii

1. Introduction 1

1.1 Facility Description 2
1.2 Measurement Plan And Equipment 3
1.2.1 Measurement Protocol 3

1.2.2 Measurement Equipment 3

1.3 The Impulse Radiating Antenna (IRA) 7
1.4 Measured Results 10

2. Summary of Important Observations 14

3. Comparisons of Transfer Functions 16

4. Operation of the Swiss IRA Near a Local Ground 19

5. Summary and Conclusions 30

6. References 32

Appendix I - Measurements of High-Power Electromagnetic Field Interaction with a Buried Facility 33

Appendix II - Illustration of EM Field Penetration into a Lossy Earth 50-51

Figures

Figure 1. The exterior view of the underground Spiez test-bed facility.....2

Figure 2. Floor plan and dimensions of the test-bed facility at the Swiss NEMP Laboratory in Spiez.....3

Figure 3. Equipment configuration for ambient noise measurements (MG-1). 4

Figure 4. Equipment configuration for transient IRA characterization (MG-2). 4

Figure 5. Equipment configuration for CW IRA characterization (MG-3). 5

Figure 6. Equipment configuration for facility measurements (MG-4), transient measurements (a) and frequency domain measurements (b). 6

Figure 7. The Swiss IRA used for the test program. 7

Figure 8. Illustration of the approximate pulser output voltage (peak value = 2.8 kV, rise time 100 ps, full width to half-max = 2 ns).....8

Figure 9. Plot of the computed on-axis IRA transient E-field (in V/m), shown for various ranges from the antenna. 9

Figure 10. The computed spectral magnitude of the IRA on-axis E-fields of Figure 9...9

Figure 11. Measured transient equivalent E-field from the IRA at a distance of 6 m from the antenna. 10

Figure 12. Transmitter and measurement locations for the test facility. 11

Figure 13. Illustration of the IRA located at the facility entrance. 12

Figure 14. Measured (equivalent) transient E-field inside the main facility door (top) and the corresponding spectral magnitude (bottom) for the IRA in the position shown in Figure 13, with the door open (data record M006.dat) and the door shut (record M0007.dat).....12

Figure 15. Measured transient current on a power line neutral inside the main facility door (top) and the corresponding computed spectral magnitude (bottom) the IRA in the position shown in Figure 13, with the door open. 13

Figure 16. Plots of the measured transfer function magnitude $|E_{meas}/V_s|$ in dB for the transmitter at location T-2 and the E-field at F-1 with the door open (top trace) and the door shut (bottom trace). 17

Figure 17. Plot of the frequency domain spectrum magnitude for the pulser output voltage of Figure 8. 18

Figure 18. Transfer function for the internal E-field at F-1 due to the IRA transmitter at location T-2, with the door open (top trace) and the door shut (bottom trace), as computed from the transient data. 18

Figure 19. Plots of measured IRA E-fields at different ranges from the antenna. 19

Figure 20. Illustration of the IRA located over a lossy earth. 20

Figure 21. Plot of the time difference in arrival of the earth-reflected pulse relative to the direct pulse. (From ref.[1]).....21

Figure 22. Plot of the surface wave attenuation function A, as a function of the parameters ρ and b. 22

Figure 23. Illustration of the various wave contributions to the total E-field from the IRA at a distance of 40 m from the IRA for an earth conductivity of σ = 0.01 S/m and a relative permittivity ε_r = 10. 23

Figure 24. Plots of the transient (top) and spectral (bottom) responses of the IRA fields for a source and observation height of 1.5 m over a lossy earth of σ = 0.01 S/m and ε_r = 10, for various distances of the observation location. ..28

Tables

Table 1. Description of measurement groups for the test program.....4
Table 2. Summary of the transient measurement results. 15

Analysis of Swiss Civil Defense Test Data

1. Introduction

In the fall of 2000, a measurement program was initiated in Switzerland to evaluate the interaction of high-power electromagnetic (HPEM) fields with Swiss civil defense facilities. These facilities are typically buried and are constructed using steel rebar and concrete to provide blast and shock hardening. They are also hardened against the nuclear electromagnetic pulse (NEMP). With the newly emerging threats to the civilian infrastructure involving higher frequency and/or faster rise-time electromagnetic (EM) environments, there is an interest in understanding the degree to which externally generated EM fields can penetrate such facilities.

This measurement program used a test-bed facility located at the NEMP Laboratory located in Spiez, Switzerland. The objective of this HEMP testing on this facility was several-fold. These were:

1. Is there a significant penetration of electromagnetic fields into an underground facility, at frequencies up to and beyond a GHz, through a 1 m earth overburden, and with concrete roofing material of the underground facility?
2. Is it possible to illuminate such large structures with localized ultra wideband transmitters, and still get interior responses that are measurable?
3. If one measures the transfer functions in time and swept CW modes, can we establish equivalence? If so, what are the implications of such equivalence in terms of measurement ease, labor and resources involved?

The testing of this facility has resulted in several interesting results – both for the EM field penetration into the facility, as well as for induced currents in power and communication lines. From these measurements, transfer functions can be calculated and compared with simple computational models. Such data are commonly available for lower-frequency HEMP excitation of facilities, but at the higher frequencies from 200 MHz to 2 GHz, data are difficult to obtain in the literature. Thus, the results from this test program are useful for understanding the HPEM field interaction with protected systems.

This note serves to summarize the results of this test program [1] and provide further analysis and discussion of the HPEM interaction with this type of facility. Section 1 of this note provides a brief overview of the test facility, the measurement equipment that were used in the test, and a sampling of the measured results. A more detailed summary of this test program is provided in Appendix I in the form of a PowerPoint presentation, which was given at the International Conference on Electromagnetics in Advanced Applications [2].

In Section 2, the important observations of this test are summarized. One of the goals of this measurement program was to measure CW transfer functions into the facility and compare them with corresponding transfer functions developed from transient data. In Section 3, the calculation of an approximate transfer function from the transient data is discussed. Unfortunately, there appears to be uncertainties in the calibration and/or presentation of the CW data, and such a comparison is not possible currently.

One of the observations made in this test program was that the E-field produced by the IRA (by itself) did not behave as expected at certain distances from the antenna. IRA calculations are performed in the absence of the lossy ground. The presence of a ground reflection of the IRA field combines with the direct wave from the source to produce a doublet-type waveform. Section 4 discusses this phenomenon in more detail and provides a simple model for computing the total IRA field for the antenna near a lossy earth. Finally, in Section 5, a brief summary is provided.

1.1 Facility Description

The building chosen for testing was a buried concrete reinforced building. It had a small aboveground concrete structure that provided protection for the stairway leading from the surface to the working area below, as seen in Figure 1.

Note that in addition to the main entrance to the facility, there were two personnel escape hatches in the back portions of the building. These are blast-hardened doors leading to tunnels to the surface. Also, there are blast doors in each compartment in the facility. Figure 2 presents the floor plan and dimensions for this facility.

Figure 1. The exterior view of the underground Spiez test-bed facility.

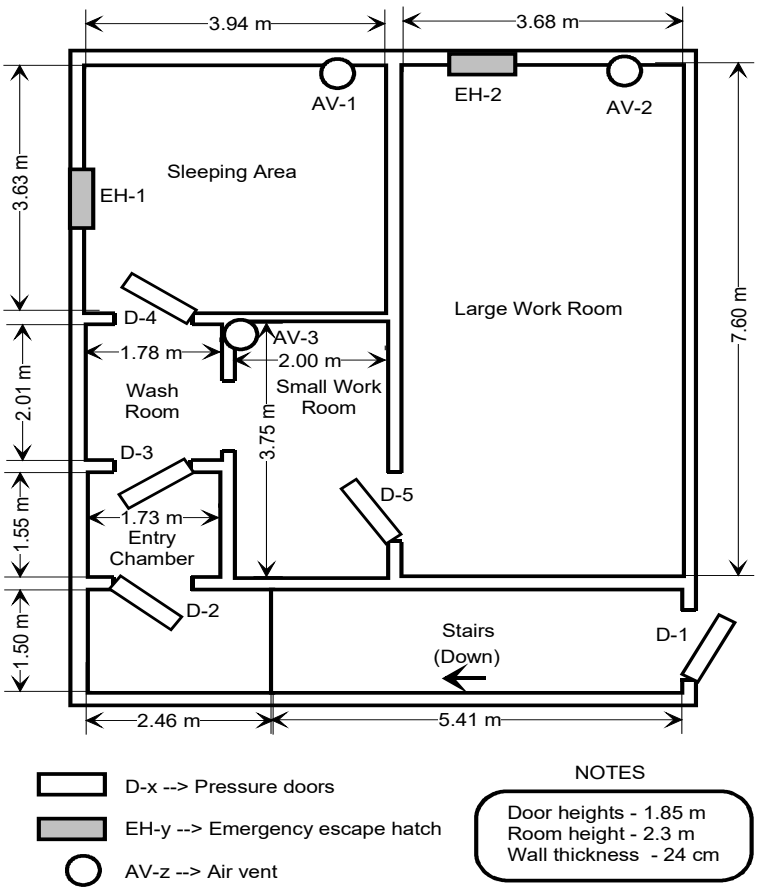

Figure 2. Floor plan and dimensions of the testbed buried facility at the Swiss NEMP Laboratory in Spiez.

1.2 Measurement Plan and Equipment

1.2.1 Measurement Protocol

The measurements were conducted during the week of October 2–6, 2000. To prepare for this test, a test plan describing the details of the facility to be tested, the required instrumentation and the testing sequences was written [3].

To meet the previously stated goals for this test, several different **m**easurement **g**roups (MG) were defined. These are summarized here in Table 1. Measurements in MG-1 though MG-3 were designed to characterize the noise environments and the EM fields produced by the IRA source, while MG-4 contained the facility measurements. More detailed descriptions of the test procedures are described in [3] and are not repeated here.

1.2.2 Measurement Equipment

For the four measurement groups in Table I, a specific equipment setup was required. Each of these setups was used to take accurate measurements for sub-nanosecond pulses for CW measurements at frequencies that could exceed 1 GHz. The equipment needed for all four measurement categories are shown in Figure 3 through Figure 6 below.

Table 1. Description of measurement groups for the test program

MG	Title	Description
1	Noise Measurements	Perform ambient signal measurement outside and inside the facility
2	IRA Transient Characterization	Characterize the Swiss IRA transmitter, via field mapping on and off boresight in time domain, using the Grant HYPS pulser.
3	IRA Frequency Domain Characterization	Characterize the CW performance of the Swiss IRA, at selected frequency in the range of 200 MHz to 5 GHz.
4	Facility Measurements	Measure the transient and CW responses in and around the test-bed facility in Spiez.

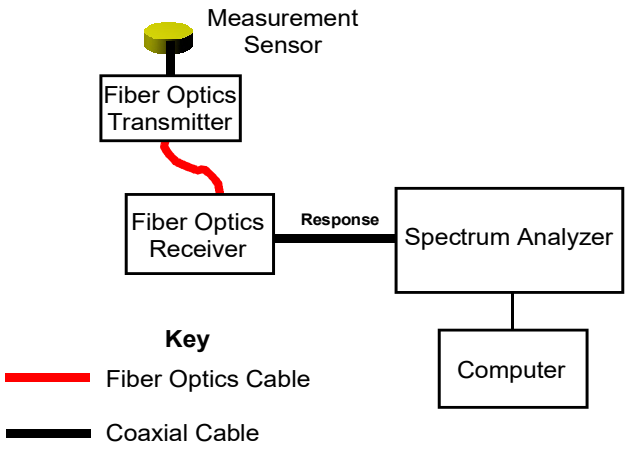

Figure 3. Equipment configuration for ambient noise measurements (MG-1).

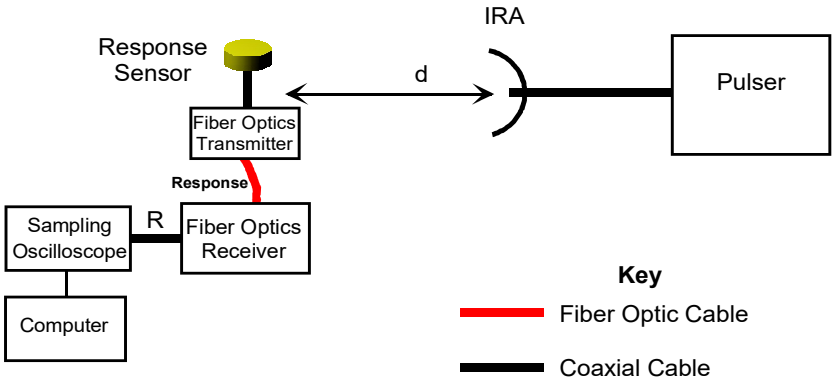

Figure 4. Equipment configuration for transient IRA characterization (MG-2).

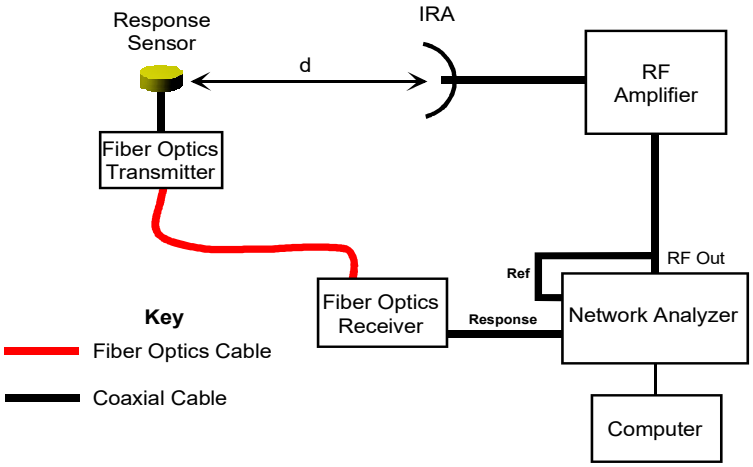

Figure 5. Equipment configuration for CW IRA characterization (MG-3).

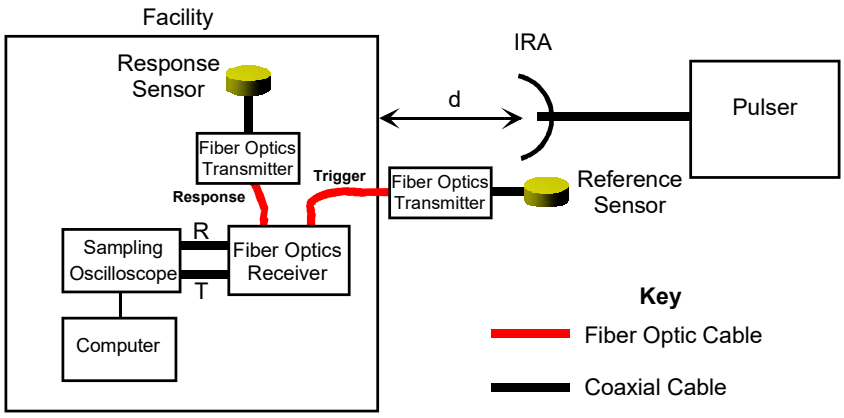

(a) Transient measurements

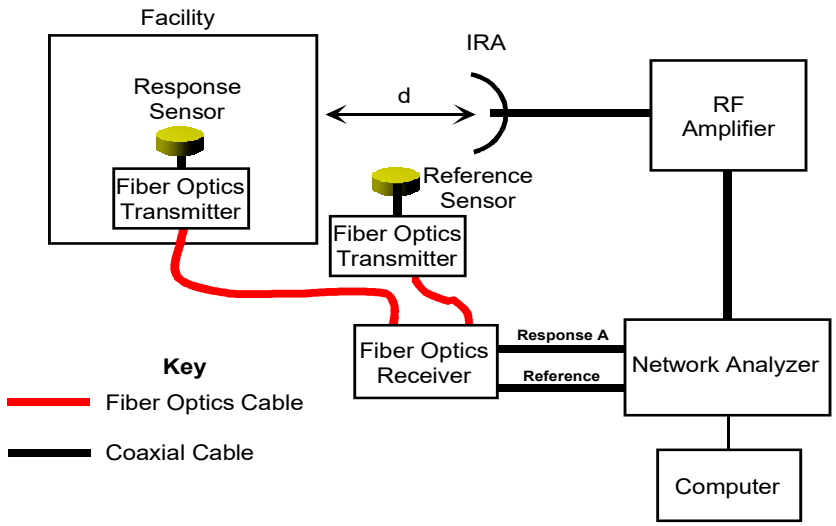

(b) Frequency domain measurements

Figure 6. Equipment configuration for facility measurements (MG-4), transient measurements (a) and frequency domain measurements (b).

1.3 The Impulse Radiating Antenna (IRA)

Both transient and CW excitations were used in these tests. For both environments, the Swiss IRA was used for the radiator, with either a commercially available pulser for the transient excitation, or a network analyzer and a broadband amplifier for the CW excitation.

This antenna uses the standard parabolic IRA design, which had been designed and built specifically for the NEMP Laboratory. It is pictured in Figure 7, and had the following parameters:

- D = Reflector antenna diameter =1.8m
- F = Focal length of the reflector = 0.48m
- F/D = Focal length / Diameter = 0.267

For this antenna, the fields are defined in a coordinate system (x, y, z), which is a rectangular coordinate system centered on the focal point; x and y are the transverse coordinates; z is the boresight axis.

a. Photo of the IRA

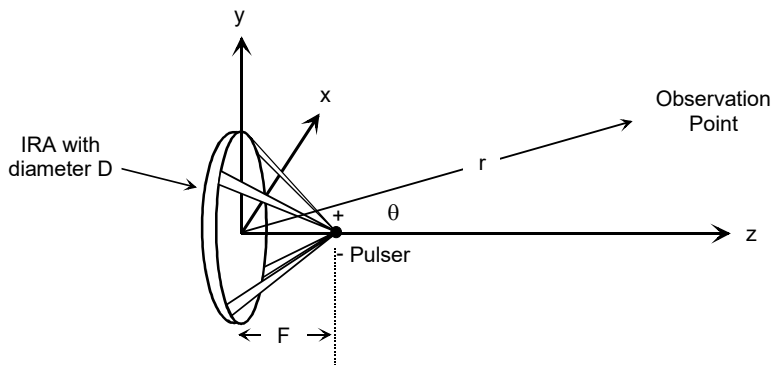

b. Illustration of the antenna

Figure 7. The Swiss IRA used for the test program.

When operated in the transient mode, the antenna was connected to the High Voltage Pulse Source (HYPS) [4]. The pertinent parameters of this commercial pulser source are summarized below:

- Peak pulser voltage = 2.8 kV
- 10-90% rise time = nominally 100 ps
- Exponential decay time = nominally 2 ns

These parameters result in a fast-rising pulsed excitation applied to the IRA, as shown in Figure 8.

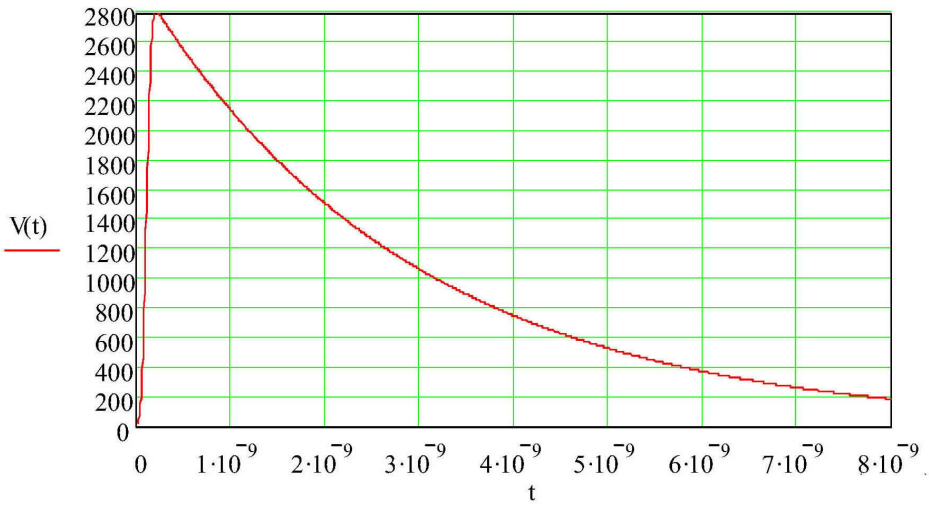

Figure 8. Illustration of the approximate pulser output voltage (peak value = 2.8 kV, rise time 100 ps, full width to half-max = 2 ns).

The pulser excitation of Figure 8 produces a radiated impulse-like waveform on the order of 300 to 1300 V/m (peak), depending on the range. Figure 9 presents the calculated transient radiated waveforms from the IRA for various observation distances. It is noted that these calculations are for an IRA by itself. In this plot, the range (in meters) is shown as the second parameter of the function argument in the y-axis. The corresponding calculated spectrum is shown in Figure 10.

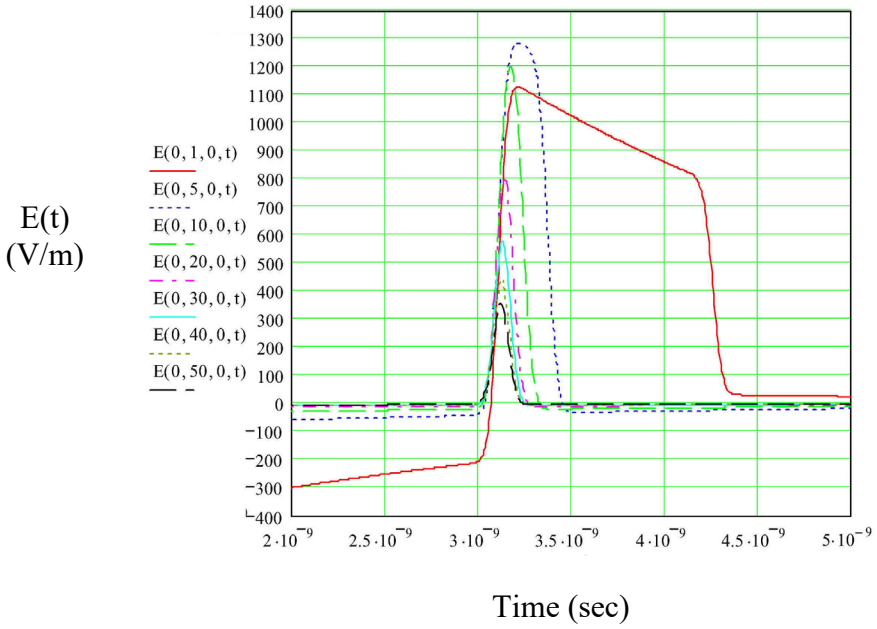

Figure 9. Plot of the computed on-axis IRA transient E-field (in V/m), shown for various ranges from the antenna.

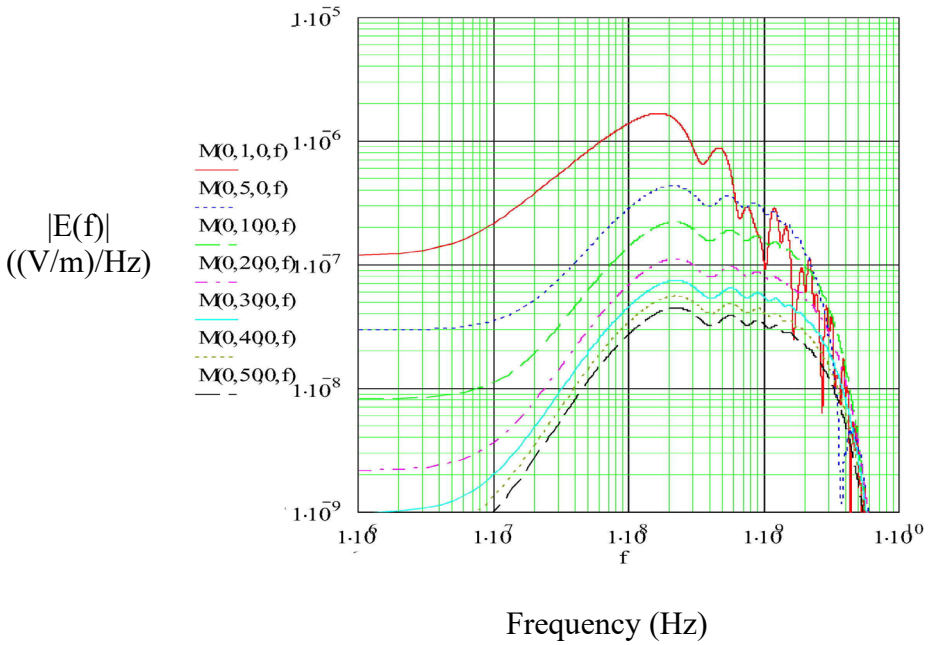

Figure 10. The computed spectral magnitude of the IRA on-axis E-fields of Figure 9.

As a verification of the calculated EM environment from this antenna, Figure 11 presents the measured transient E-field from the IRA at a distance of 6 meters from the radiator. As noted from a comparison with Figure 9, the agreement between the theoretical and experimental results is reasonable. Additional plots of measured IRA E-fields as a function of range from the antenna, together with theoretical calculations are provided in Section 4.

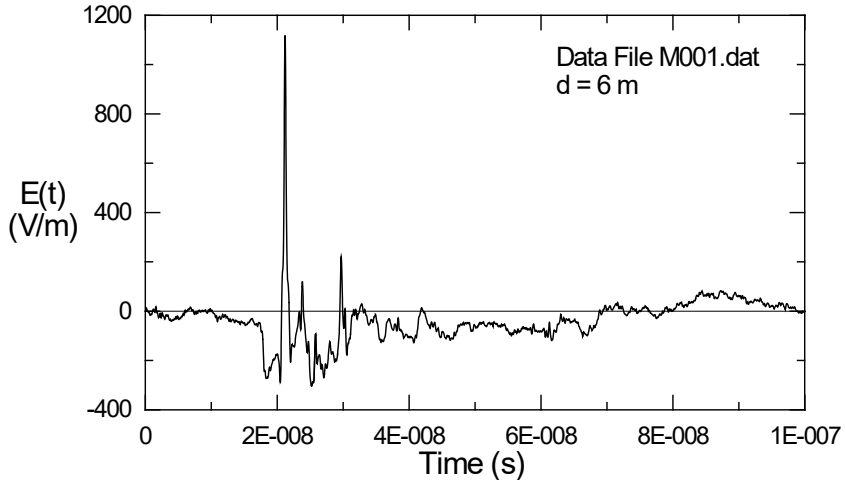

Figure 11. Measured transient equivalent E-field from the IRA at 6 m from the antenna.

1.4 Measured Results

In this measurement program several different antenna locations and observation points for EM fields and induced wire currents were made. These locations are indicated in Figure 12, where the external excitation locations of the IRA source are indicated by the symbol (T). Of course, the transmitter is located above the ground. Within the facility, various field test points are defined, and these are shown by the (F) symbol. In addition, the locations of the current measurements on selected cables within the facility are indicated in by the (C) symbol.

For a more complete description of these measurements in this note, see [1].

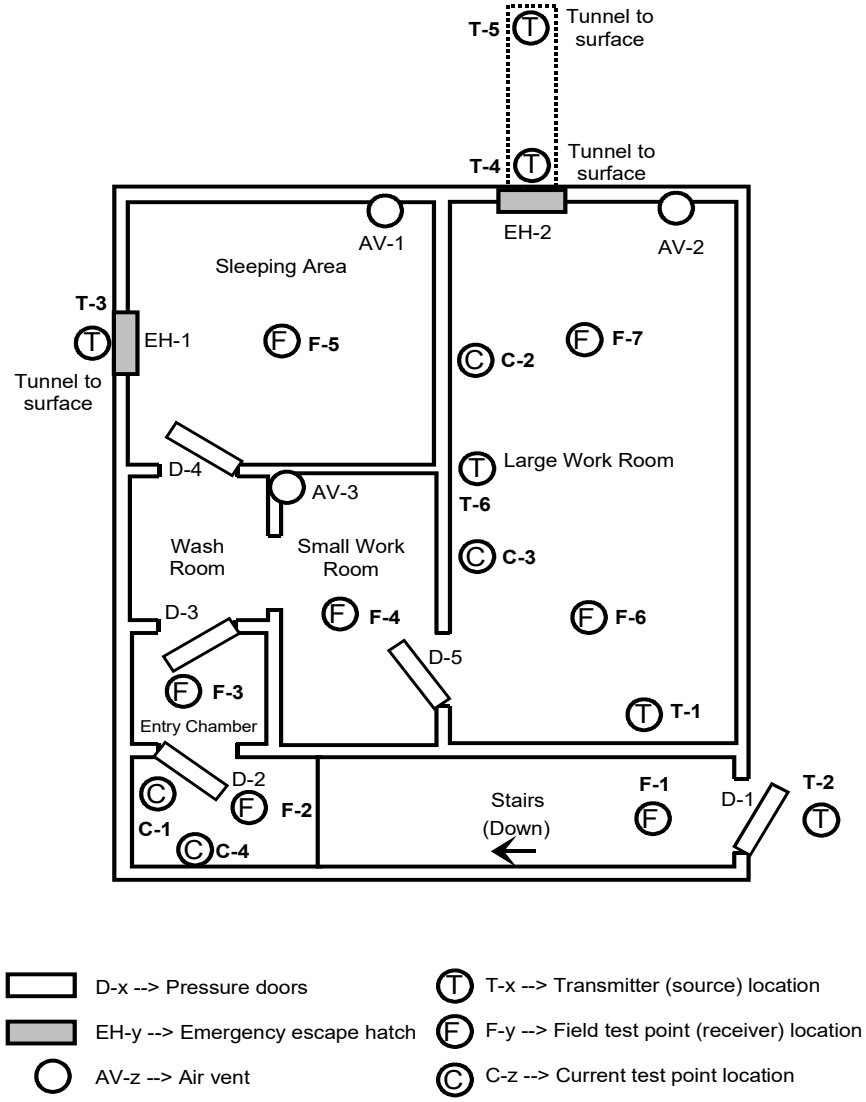

Figure 12. Transmitter and measurement locations for the buried test facility.

Figure 13 illustrates one of the first facility measurements made, with the IRA source located at the main entrance of the shelter. Both the door-open and door-closed configurations were used. The measured transient and computed spectral densities for both the door open and door shut are shown in Figure 14. Note that in most cases, the physically measured quantity was the B-field, and this was converted to an "equivalent" E-field using the free-space impedance.

Figure 13. Illustration of the IRA located at the facility entrance.

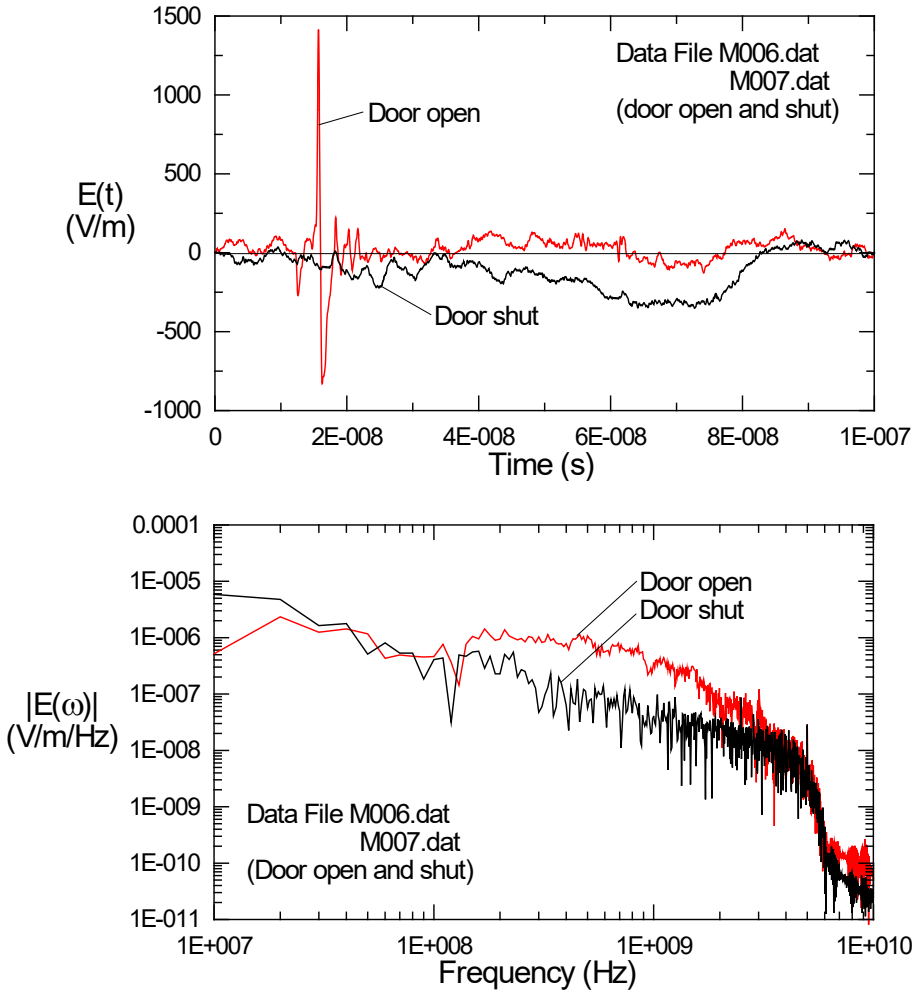

Figure 14. Measured (equivalent) transient E-field inside the main facility door (top) and the corresponding spectral magnitude (bottom) for the IRA in the position shown in Figure 13, with the door open (data record M006.dat) and the door shut (record M0007.dat).

Transient current measurements on power and telephone lines were also made during this test program. At the bottom of the stairs in the facility entrance shown in Figure 13 was a power system interconnection panel, where a ground wire was instrumented with a current probe. The measured transient current in this wire was measured, and the response for the door-open case is shown in top of Figure 15. The computed spectral density magnitude for this current is shown in bottom part of this figure.

For a more complete description of the measured data, consult ref.[1] or the presentation material in Appendix I.

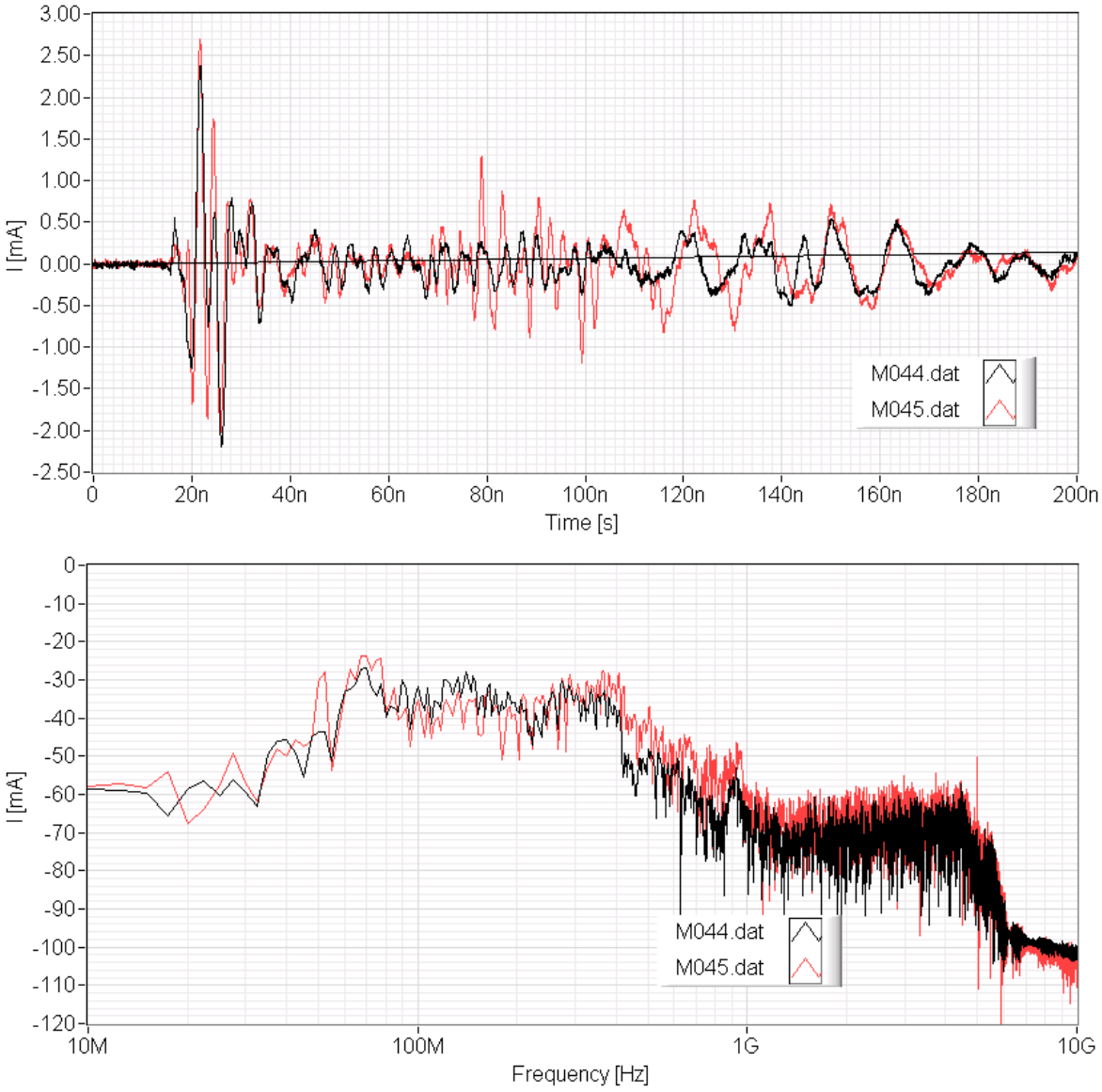

Figure 15. Measured transient current on a power line neutral inside the main facility door (top) and the corresponding computed spectral magnitude (bottom) the IRA in the position shown in Figure 13, with the door open.

2. Summary of Important Observations

This section summarizes the results of the transient measurements performed on the buried facility in Spiez. The briefing in Appendix I of this report illustrates the various response waveforms to be discussed in this context.

The IRA source used to illuminate the facility had a transient 2.8 kV pulser as a source, and it was seen to produce an incident peak E-field environment at 6 meters of about 1.1 kV/m. This resulted in ($r\ E_{far}/V$) of 2.35 = (6 x 1.1/2.8). This excitation field penetrated the facility, producing, in some cases, both an internal field distribution, and induced currents on internal telecom and power.

For some of the measurements, when the IRA source was illuminating one portion of the facility and internal fields were measured in a different, non-illuminated room, the internal EM fields were too small to be observed. However, in other cases where the external IRA antenna directly illuminated an internal room of the facility through walls, or through the earth overburden and facility roof, internal E-fields were measurable.

For example, with the IRA placed at location T-1 of Figure 12 and fields measured at location F-1, the concrete wall with rebar provides an attenuation of the peak equivalent E-field[1] of approximately 10.7 dB.

Moving the IRA to T-2 and measuring the equivalent E-field variation as the internal field observation point moves from F-1 to F-2 shows that there is a 23dB field reduction with distance. (A simple $1/r$ scaling gives only 17 dB, indicating that there is a bit more attenuation for the waves propagating in the entryway "tunnel"). In addition, there is significant ringing in measured response at F-2. These measurements were made with the front door both open and shut. It was noted that the field reduction due to shutting door is significant.

Turning the corner to observation location F-3 significantly reduces the response, and for this T-2 transmitter location, it was found that other internal E-fields were not measurable.

However, significant fields inside the facility were possible with illumination from the top of the facility through the earth overburden. For the external antenna at location T-7 and fields being measured in the large work room at location F-7, internal fields up to 80 V/m were observed, suggesting that the peak E-field attenuation into the building is ~ 25 dB.

With the external antenna at T-4 and fields measured either in the room at F-7, or just outside the metal grate on the blast door to the escape hatch, it was found that the metal grate will significantly reduce internal fields. The conclusion is that more of the internal EM fields in the workroom diffuse through the facility roof and overburden than enter through the tunnel and grates.

Regarding the induced currents on internal cables, it was found that in many cases, a well-defined current could be measured. Moreover, we noted that these responses were generally not affected by the front door being open or shut. This observation led to the

[1] Recall that the physical EM field quantity measured is the H-field with an H-dot sensor. The results are presented in the form of an equivalent E-field, determined from the free-space impedance, as $E_{eq} = Z_o\ H_{meas}$.

conclusion that EM field coupling to external buried cables is probably the means of producing the internal current responses.

On the telephone system, a rather large current response (~ 1 0 ma peak) was noted at observation location C-2 when the transmitter was located at T-6. This response is about 2 times that for the excitation at T-2. In both cases, there is a very dramatic high-frequency fall-off of the response spectrum for $f > 300$ MHz, which is attributed to the large attenuation of the EM field at the higher frequencies. Appendix II presents computed plots of the E-field attenuation, as a function of frequency, for different burial depths for a typical earth. In this appendix, it is clear that the high frequencies of the IRA source do not propagate well.

As in the telephone system current measurements, well-defined waveforms are noted on the power system; however, the antenna placement does not seem to be as important for these responses. The induced currents on the power system seem to be largest at low frequencies, where the antenna beam is not very directional. For the source at location T-6, the power system response is less than for the T-2 excitation (a factor of 10 smaller). This observation is unlike the telephone measurements, which had a larger response for the T-6 excitation.

Table 2 summarizes the above observations for the transient responses.

Table 2. Summary of the transient measurement results.

Response and Location	Peak Response
Peak internal E-fields in stair well bottom	**100 V/m** (Main door open) **30 V/m** (Main door closed)
Peak internal E-fields in chamber next to stair well bottom	**50 V/m** (Main door open)
Peak E-fields in facility interior with propagation through overburden	**80 V/m***
Current on telecom lines	**5-10 mA**, depending on transmitter location
Peak current on power ground/neutral phase conductor	**3 mA** for IRA illuminating switching panel **0.3 mA** for IRA illuminating facility through overburden

* The 80 V/m electric field measured inside the facility for a 1.1 kV/m transient peak field appears to be high. We do not know how such a high field got into the system interior as the coupling paths have not been analyzed. It is likely that the exterior fields couple to some conductor outside the busied facility and bring the EM energy into the interior space. Currents that penetrate the facility then radiate in the interior space, producing fairly high fields. Only an EM topological analysis can determine such coupling paths.

3. Comparisons of Transfer Functions

One of the goals of this test was to examine the measured transient and frequency responses to compare the EM field transfer functions into the facility. Results from this study are reported in the present section.

In the CW measurement program, the frequency domain transfer function was measured directly using the equipment set-up of Figure 6b. As previously discussed, this transfer function was between the applied pulser voltage V_S, and the equivalent E-field at a selected point in the facility. As such, the transfer function has the basic definition

$$T(\omega) = \frac{E_{meas}(\omega)}{V_s(\omega)} \quad (\text{in units of 1/m}) \tag{1}$$

where ω is the angular frequency $\omega = 2\pi f$. For these frequency domain measurements, the pulser voltage spectrum was measured using a directional coupler connected to the antenna output, and as such, the actual antenna excitation voltage source was used as the reference signal.

To illustrate a sample transfer function, consider Figure 16a, which shows the quantity $|E_{\text{meas}}/V_{\text{s}}|$ (in dB), for the transmitter at location T-2 and the E-field at F-1, with the main facility door open and shut, as reported in ref. [1]. Note that in this plot, the B-dot sensor calibration, together with the integration of the derivative nature of the sensor has not been considered. Thus, the transfer function is on the order of – 80 dB or so.

Using the equivalent area of the B-dot sensor (A_{eq} = 2 x 10^{-5} m^2) and taking into account the 8 dB attenuation of the balun and a 6 dB gain in the fiber optics transducer, the transfer function data in Figure 16a has been corrected, and the results are presented in part b of the figure. This has been done for both the door open and door shut cases.

To develop a transfer function from the transient results, the measured transient responses (Figure 14a in this case) must be Fourier transformed and then divided by the spectrum of the transient pulser excitation. For the case under discussion here (transmitter at T-2 and E-field at F-1), Figure 14b has presented this spectrum.

The difficulty in constructing the transfer function from these transient measurements is that the actual transient voltage exciting the IRA was not measured. The reference sensor for the transient measurements was a small surface mount H-field probe (discussed in [1]), and this was used principally as a trigger for starting the measurement recording. Thus, there is insufficient data to obtain a transfer function from just the transient measurements.

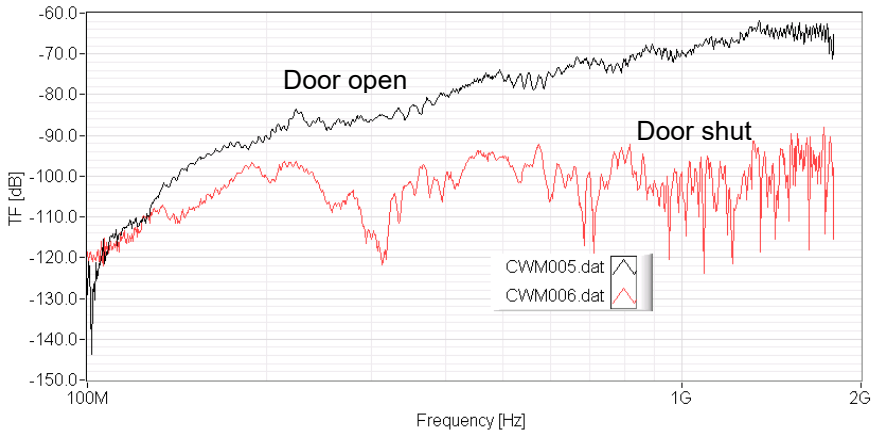

a. Unprocessed measured transfer function data.

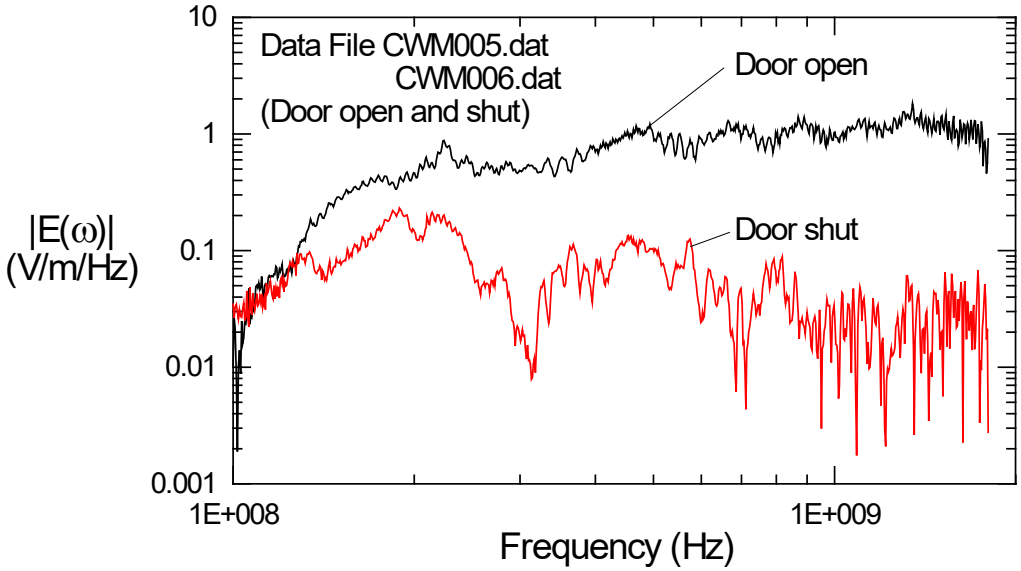

b. Transfer function obtained using the measurement chain parameters.

Figure 16. Plots of the measured transfer function magnitude $|E_{meas}/V_s|$ in dB for the transmitter at location T-2 and the E-field at F-1 with the door open (top trace) and the door shut (bottom trace).

It is possible, however, to obtain an *approximate* transfer function by dividing the spectra of Figure 14b by the Fourier spectrum of the analytical excitation shown in Figure 8. The magnitude plot of this approximation to the actual pulser spectrum is shown in Figure 17, and the resulting approximate transfer function obtained in this manner is presented in Figure 18.

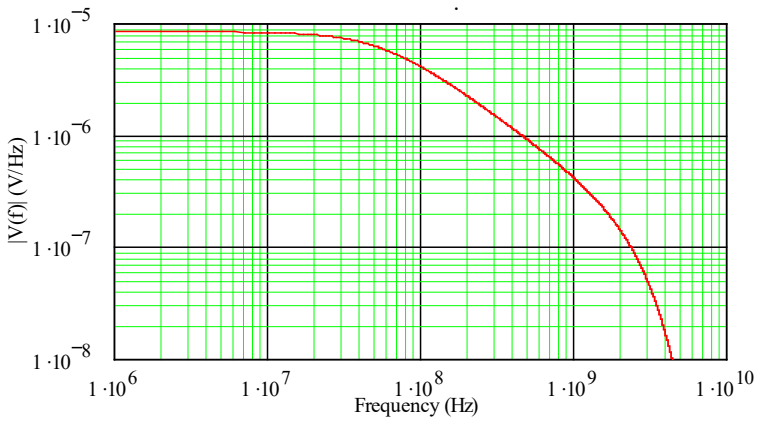

Figure 17. Plot of the frequency domain spectrum magnitude for the pulser output voltage of Figure 8.

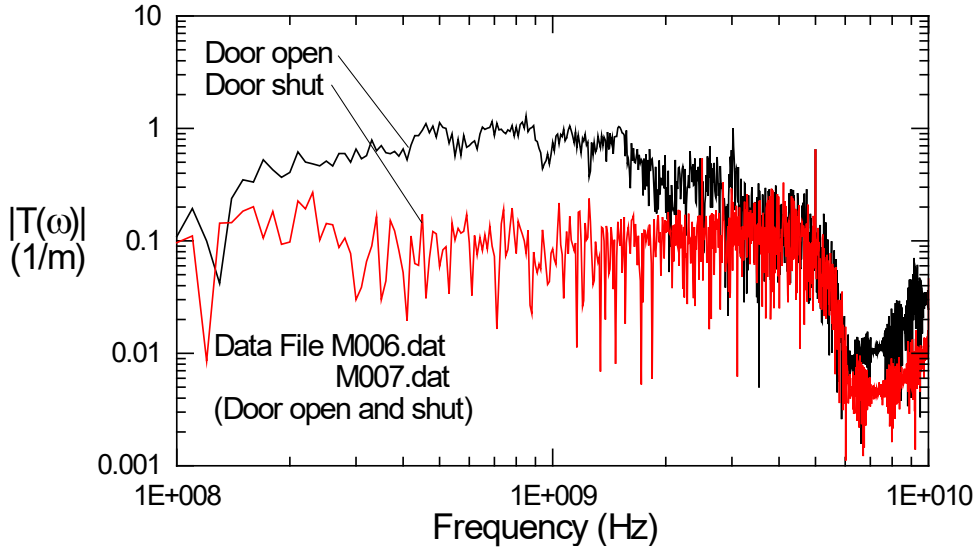

Figure 18. Transfer function for the internal E-field at F-1 due to the IRA transmitter at location T-2, with the door open (top trace) and the door shut (bottom trace), as computed from the transient data.

The transfer function data shown in Figure 18 is very similar, both in shape and in amplitude, to the CW-measured transfer function of Figure 16 over the frequency range of 100 MHz to 2 GHz. Above 1 GHz, the CW measurements were truncated, so a comparison of these results cannot be made. Nevertheless, this example serves to confirm the equivalence of the transient and CW measurement approaches for evaluating the transfer function.

4. Operation of the Swiss IRA Near a Local Ground

One of the interesting observations in the measured data in this test was that the IRA field changes its wave shape as the distance from the antenna to the observation location increases. Close to the antenna, the wave shape is similar to that given in Figure 9, but as the distance increases, the waveform becomes more like a doublet – having a positive and negative peak of comparable magnitudes.

As an example of this effect, Figure 19 plots the measured IRA waveform from distances ranging from 10 m to 50 m along the boresight of the antenna.

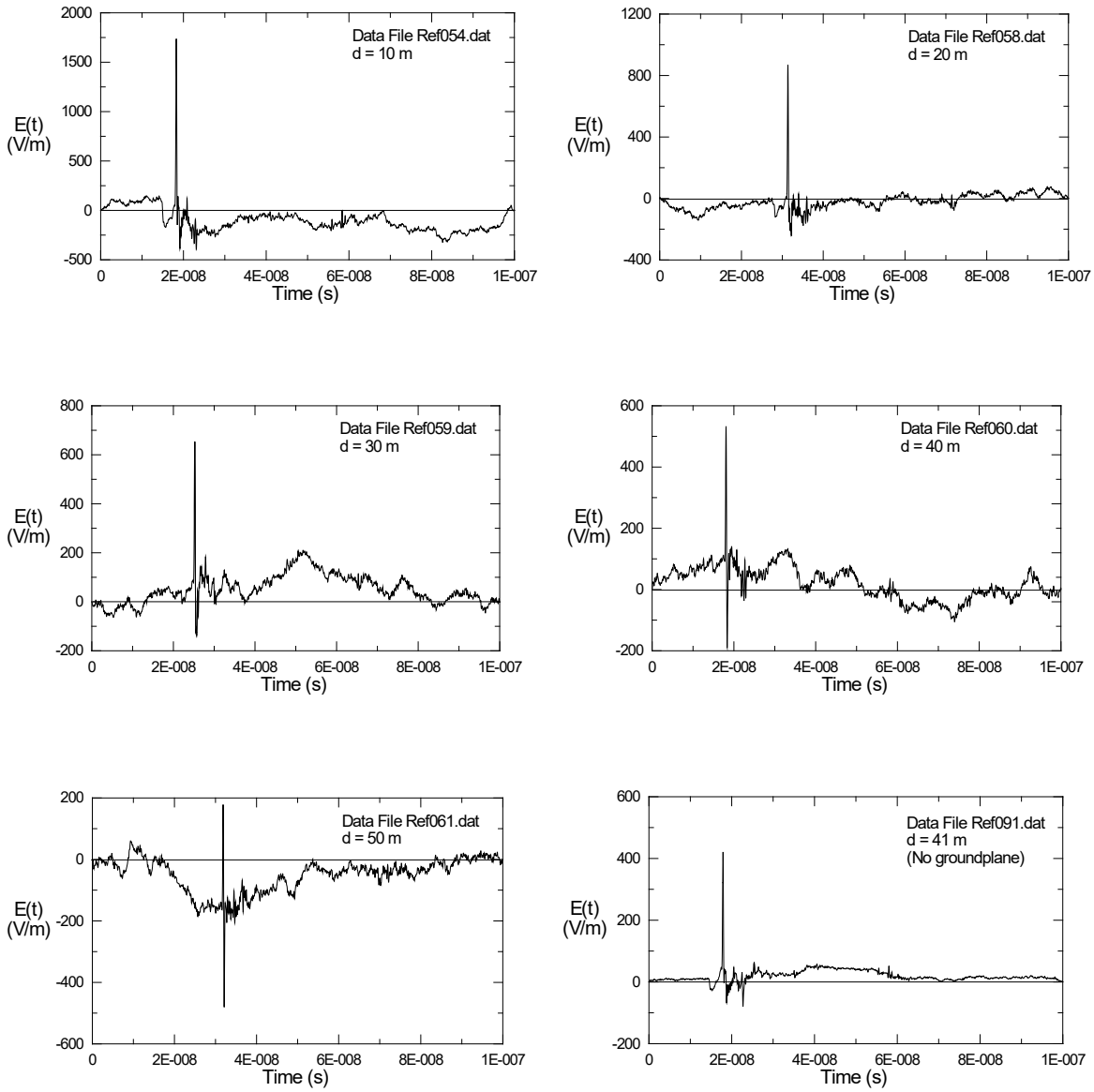

Figure 19. Plots of measured IRA E-fields at different ranges from the antenna.

For the first five plots in Figure 19, the height of both the IRA and the observation point was approximately 1.5 m over the earth. The last data plot (labeled Ref 091.dat) was at a distance of 41 m from the antenna, but with the observation point well above the earth (in a second-story window of a building) so that the earth reflection is negligible.

In the data of Figure 19, we note that within the range of 20 to 30 m from the antenna, the character of the waveform begins to change. As noted in ref. [1], this is due to the nearly simultaneous arrival of an earth-reflected waveform component, which is portrayed in Figure 20.

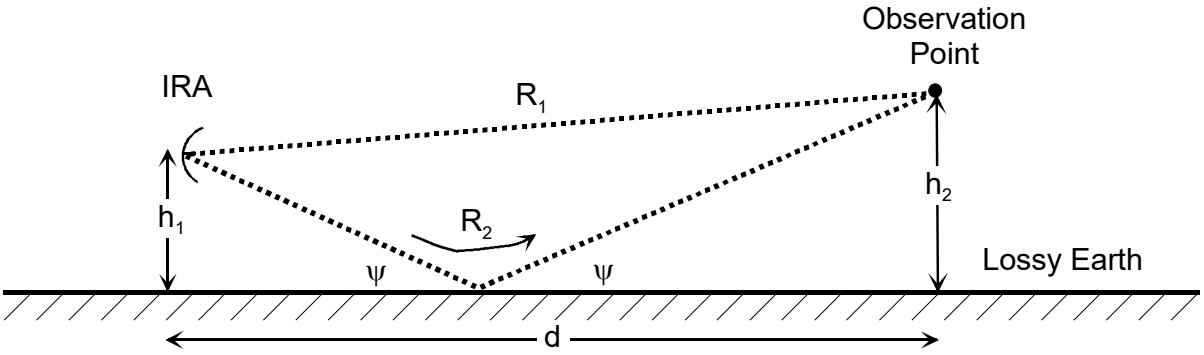

Figure 20. Illustration of the IRA located over a lossy earth.

From Snell's law, the angle of incidence is equal to the angle of reflection, and this can be expressed from the geometry of Figure 20 as

$$\psi = \tan^{-1}\left(\frac{h_1 + h_2}{d}\right). \tag{1}$$

Moreover, the two distances R_2 and R_1 are given as

$$R_2 = d\left[\left(\frac{h_1 + h_2}{d}\right)^2 + 1\right]^{1/2} \quad and \quad R_1 = d\left[\left(\frac{h_1 - h_2}{d}\right)^2 + 1\right]^{1/2}. \tag{2}$$

In examining Figure 20 it is apparent that the earth-reflected field will arrive at the observer at a time slightly later than the direct signal from the antenna (along path R_1). This differential time is given very simply as

$$\Delta t = \frac{R_2 - R_1}{c}, \tag{3}$$

and a plot of this time difference is provided in Figure 21.

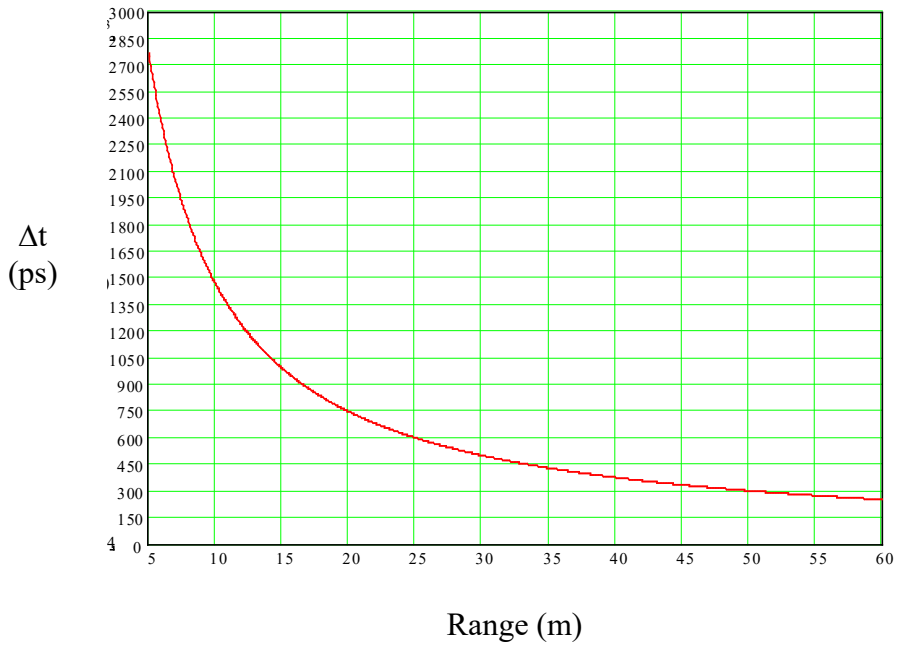

Figure 21. Plot of the time difference in arrival of the earth-reflected pulse relative to the direct pulse. (From ref.[1]).

This arrival time information helps to understand the behavior of the fields in Figure 19, but it does not tell the complete story, as the strength of the earth-reflected field is modified by the electrical properties of the earth. Moreover, as discussed in [5] there can be a surface wave contribution to the field in addition to the direct and reflected waves.

For the simple case of a vertically polarized wave[2], the direct, reflected and surface wave components can be approximated as

$$\frac{E}{E_o} \cong \quad 1 \quad + R_v \; e^{-j\Delta\phi} \quad + \quad (1 - R_v)\, A\, e^{-j\Delta\phi} \tag{4}$$

where R_v is the Fresnel reflection coefficient for vertical polarization given in [5] as

$$R_v(\Psi, f) = \frac{\varepsilon_r\left(1+\frac{\sigma}{j\omega\varepsilon}\right)\sin\Psi - \left[\varepsilon_r\left(1+\frac{\sigma}{j\omega\varepsilon}\right) - \cos^2\Psi\right]^{1/2}}{\varepsilon_r\left(1+\frac{\sigma}{j\omega\varepsilon}\right)\sin\Psi + \left[\varepsilon_r\left(1+\frac{\sigma}{j\omega\varepsilon}\right) - \cos^2\Psi\right]^{1/2}}, \tag{5}$$

where ω is the angular frequency $\omega = 2\pi f$, and the phase factor $\Delta\phi$ is expressed in terms of the path differences as

[2] The IRA in its normal configuration produces an E-field that is principally vertically polarized.

$$\Delta\phi = \frac{\omega}{c}(R_2 - R_1) = \frac{\omega d}{c}\left\{\left[\left(\frac{h_1+h_2}{d}\right)^2 + 1\right]^{1/2} - \left[\left(\frac{h_1-h_2}{d}\right)^2 + 1\right]^{1/2}\right\} \tag{6}$$

In Eq.(4), the factor A is an attenuation factor of the surface wave, which can be computed rigorously from Eq.(4.71) of ref.[5]. To facilitate this calculation, it is convenient to introduce the following parameters

$$b = \tan^{-1}\left[\frac{\omega\varepsilon_o}{\sigma}(\varepsilon_r + 1)\right] \tag{7a}$$

and

$$\rho \cong \left|\frac{\omega\varepsilon_o}{\sigma}\,\frac{\pi R}{\lambda}\,\cos(b)\right| \tag{7b}$$

where ρ is referred to as the "numerical distance" between the source and observation point. Figure 22 plots the resulting attenuation factor A as a function of ρ and b for the surface wave, for source and observation points close to the earth surface.

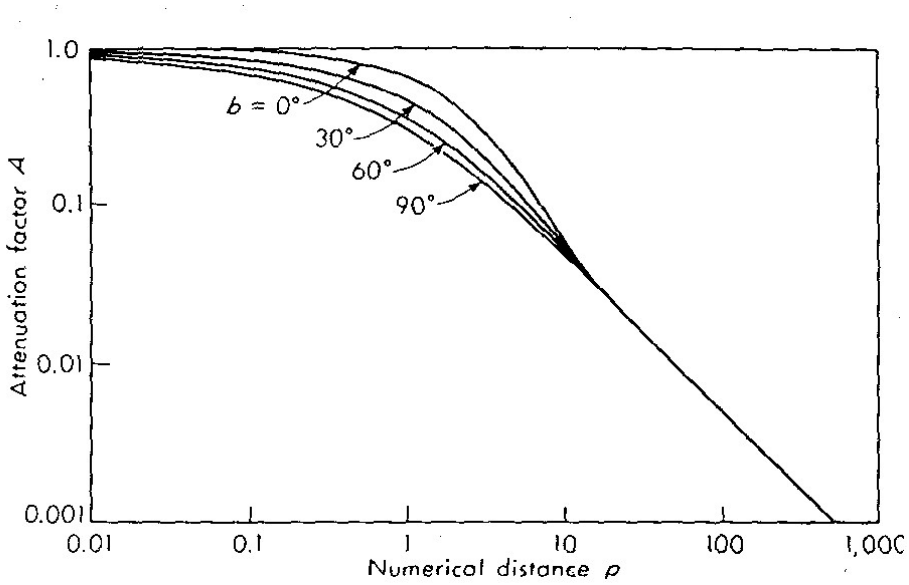

Figure 22. Plot of the surface wave attenuation function A, as a function of the parameters ρ and b.

To examine the effect that the earth has on the IRA field, a simple IRA model based on the analysis of ref. [6] has been developed. This model involves computing the incident TEM field produced by the 4-arm transmission line feed structure shown in Figure 7b over the circular aperture, and integrating over this spatial distribution to find the radiated field at the observation point. In doing this, the pre-pulse radiation contribution to the field, which is due to the backward radiation from the source and feed structure, is neglected.

In order to illustrate the behavior of the direct, earth-reflected and surface wave contribution to the total E-field at the observation point, consider the case of the observation

point located at 40 m from the IRA. Assuming an earth conductivity of $\sigma = 0.01$ S/m and a relative permittivity $\varepsilon_r = 10$, Figure 23 presents the wave contributions to the total E-field. As seen in this figure, the surface wave contribution (in blue) is not very important compared with the contributions from the direct and reflected waves, and thus, it could have been omitted in this case.

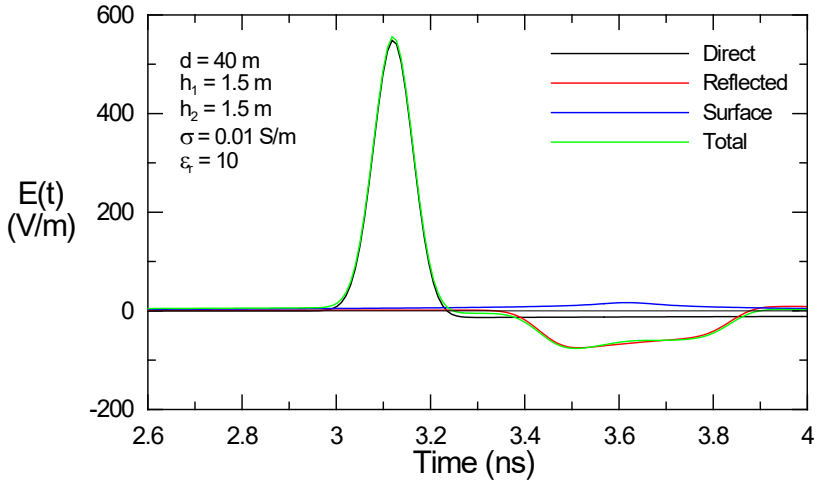

Figure 23. Illustration of the various wave contributions to the total E-field from the IRA at a distance of 40 m from the IRA for an earth conductivity of $\sigma = 0.01$ S/m and a relative permittivity $\varepsilon_r = 10$.

It is interesting to note that the reflected component to the total field in negative in this case. As discussed in [1], for large angles of incidence (or for a perfectly conducting ground) the reflection coefficient is positive, and this results in a positive earth-reflected field. (See Figure 24a). However, for shallow angles of incidence on a lossy earth, there is a sign reversal of the real part of the reflection coefficient and this causes the earth-reflected wave to reverse in sign. Consequently, as the range of the observation location increases, the angle of incidence becomes smaller and the total waveform begins to have a large negative spike due to the reflected field. This effect is noticeable in Figure 24, where the range is allowed to vary from 5 to 100 m from the IRA.

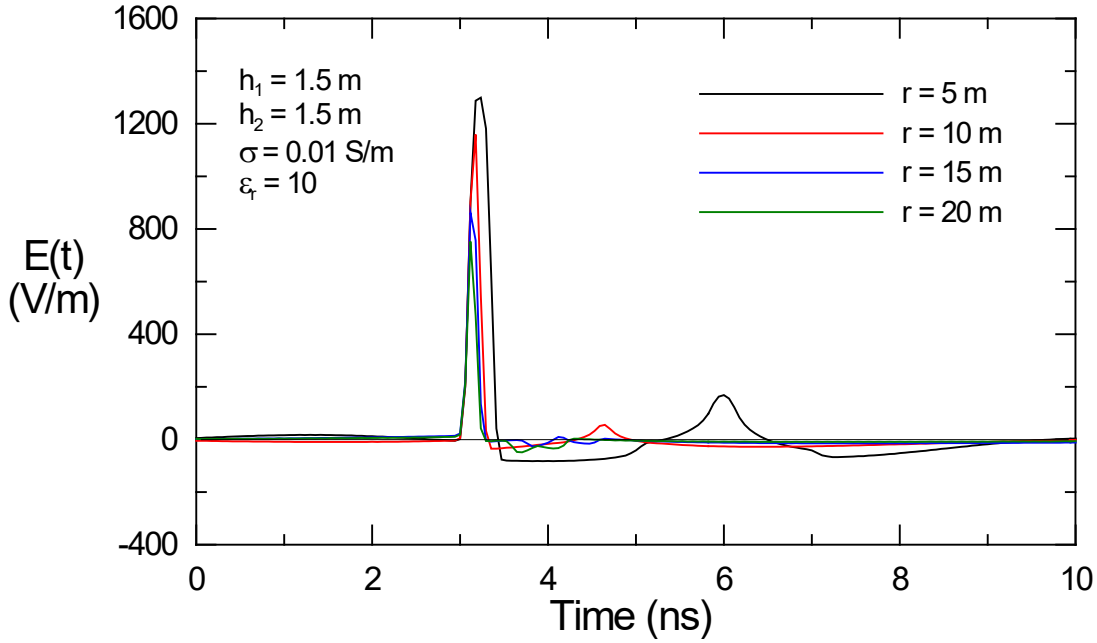

a. Transient response for d = 5 to 20 m

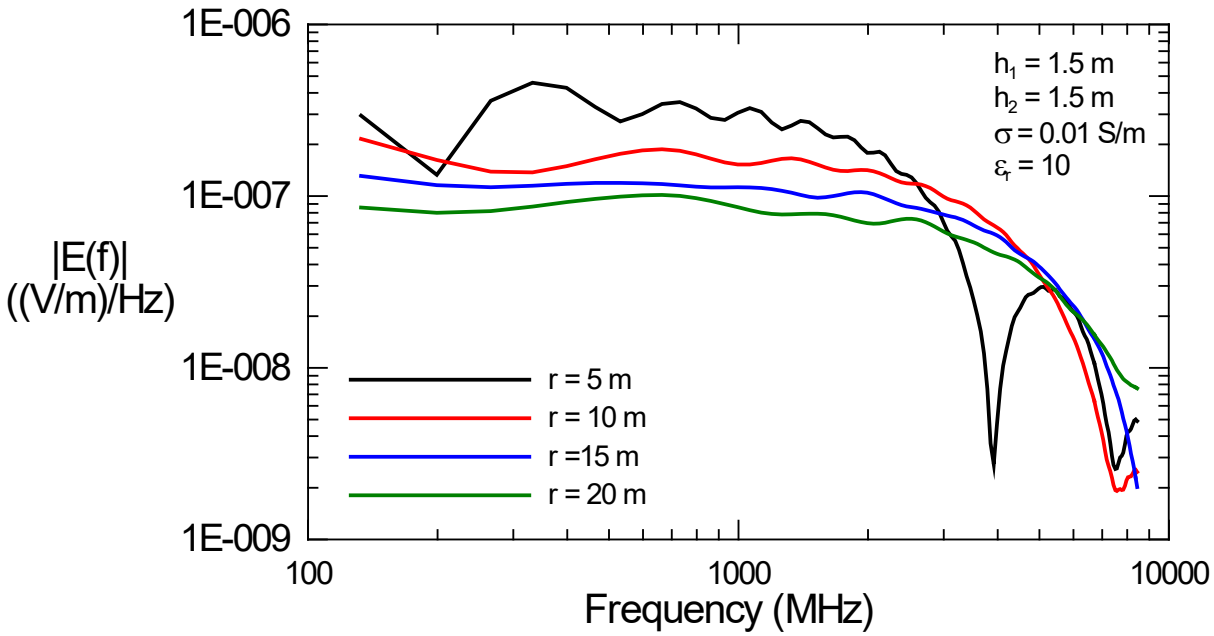

b. Spectral response for d = 5 to 20 m

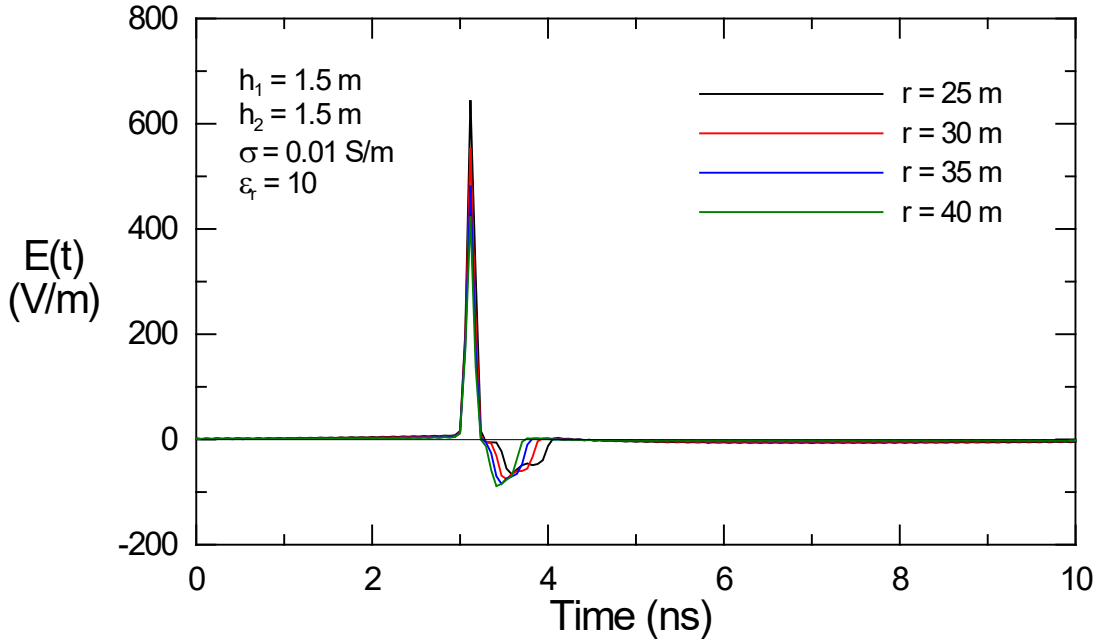

c. Transient response for d = 25 to 40 m

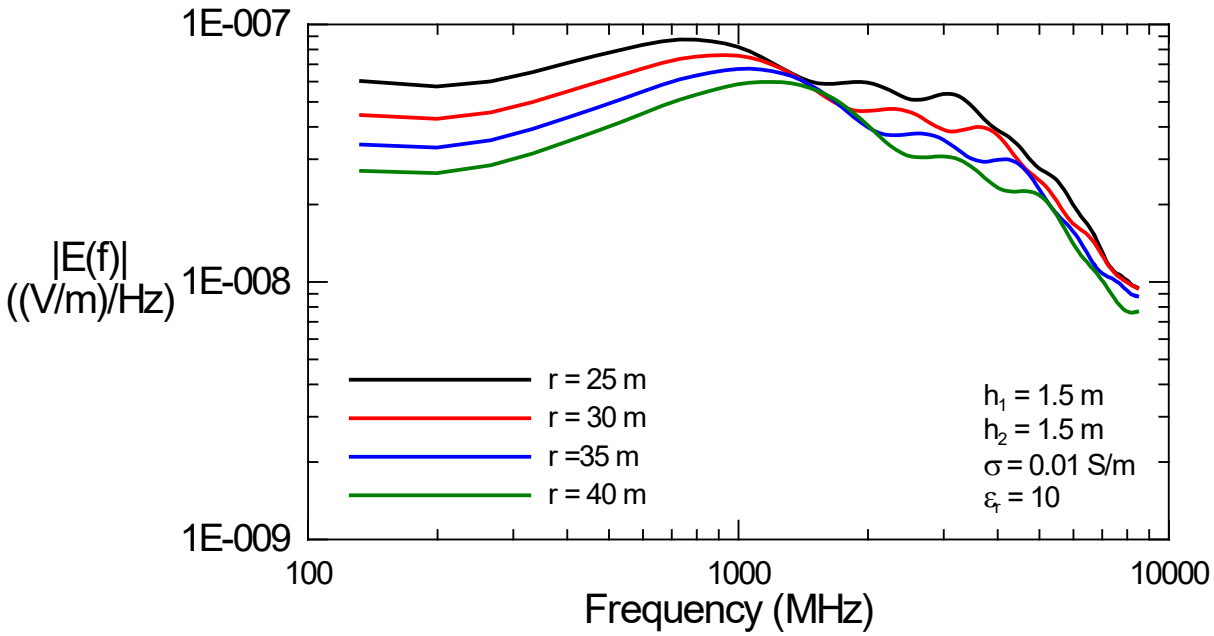

d. Spectral response for d = 25 to 40 m

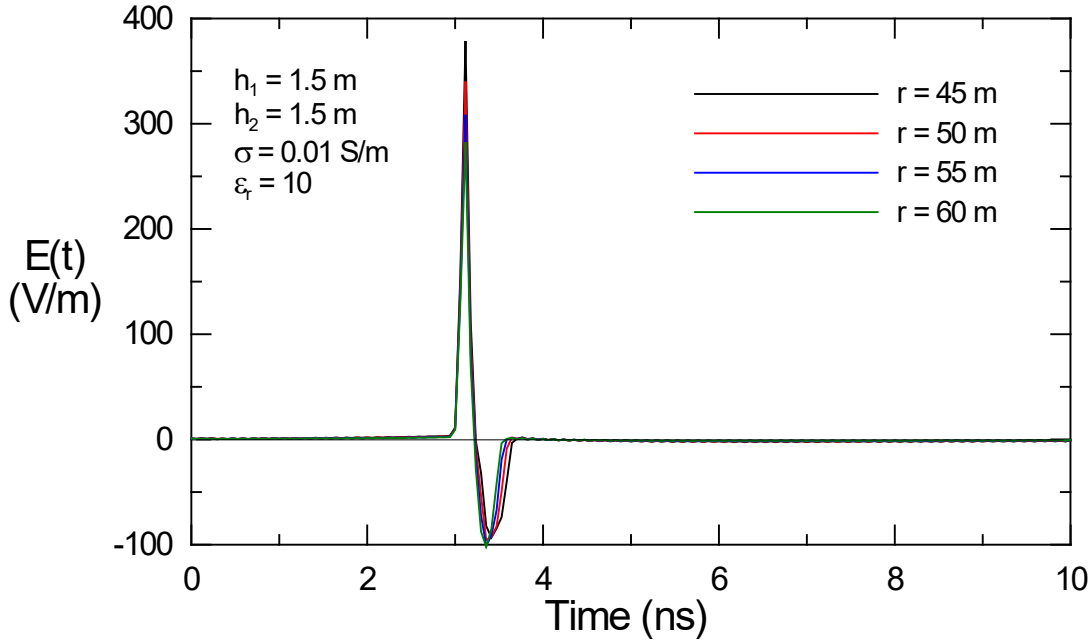

e. Transient response for d = 45 to 60 m

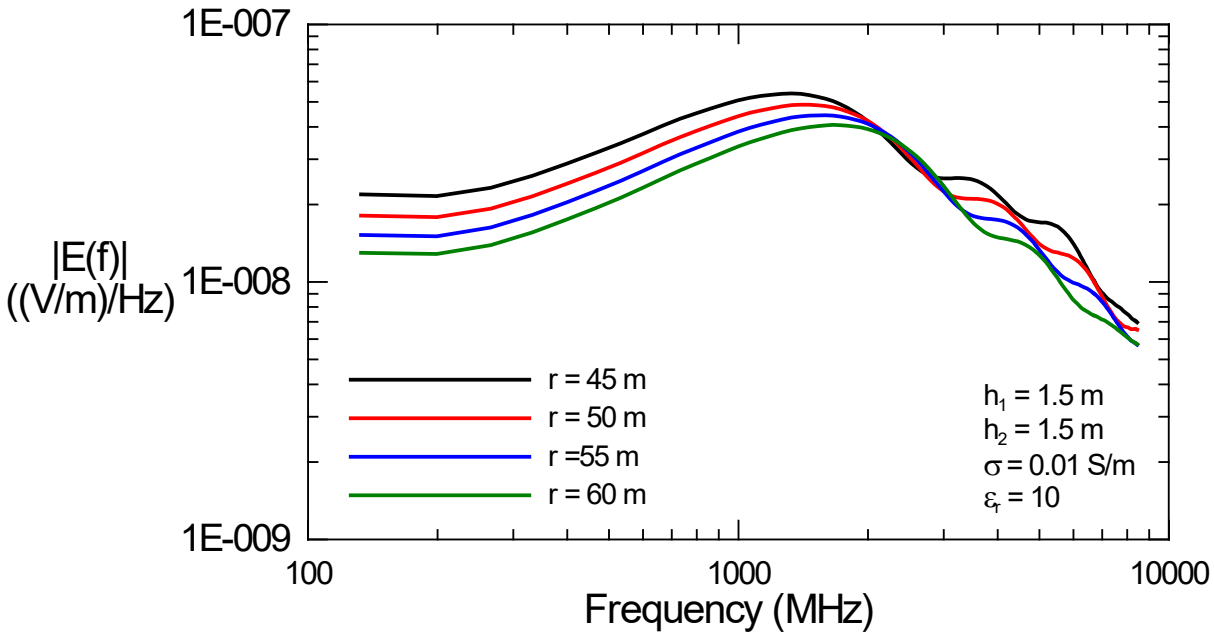

f. Spectral response for d = 45 to 60 m

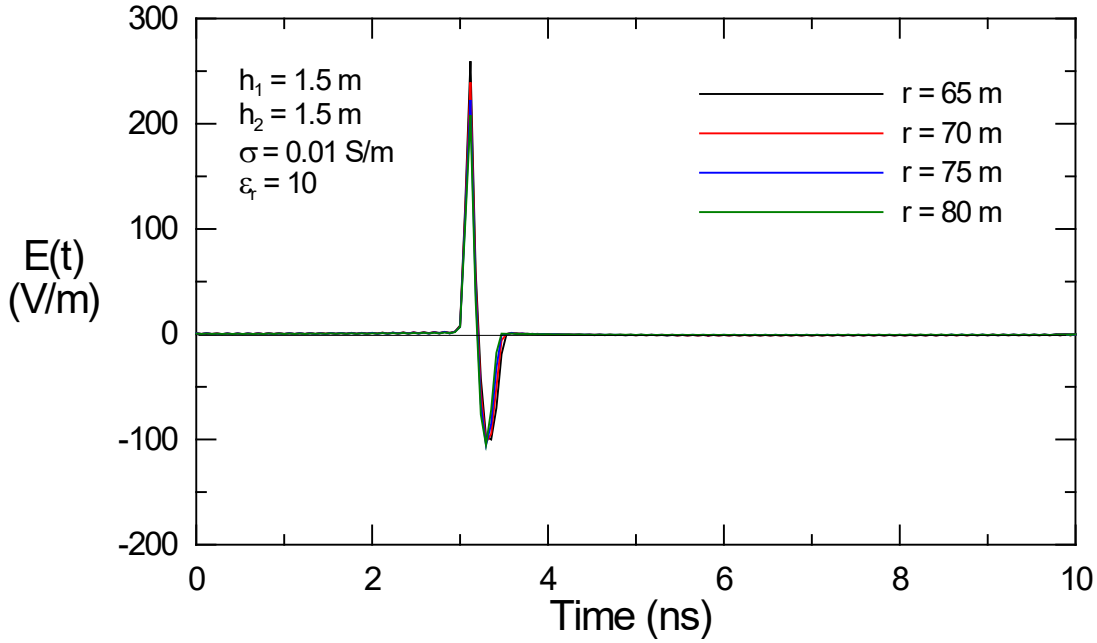

g. Transient response for d = 65 to 80 m

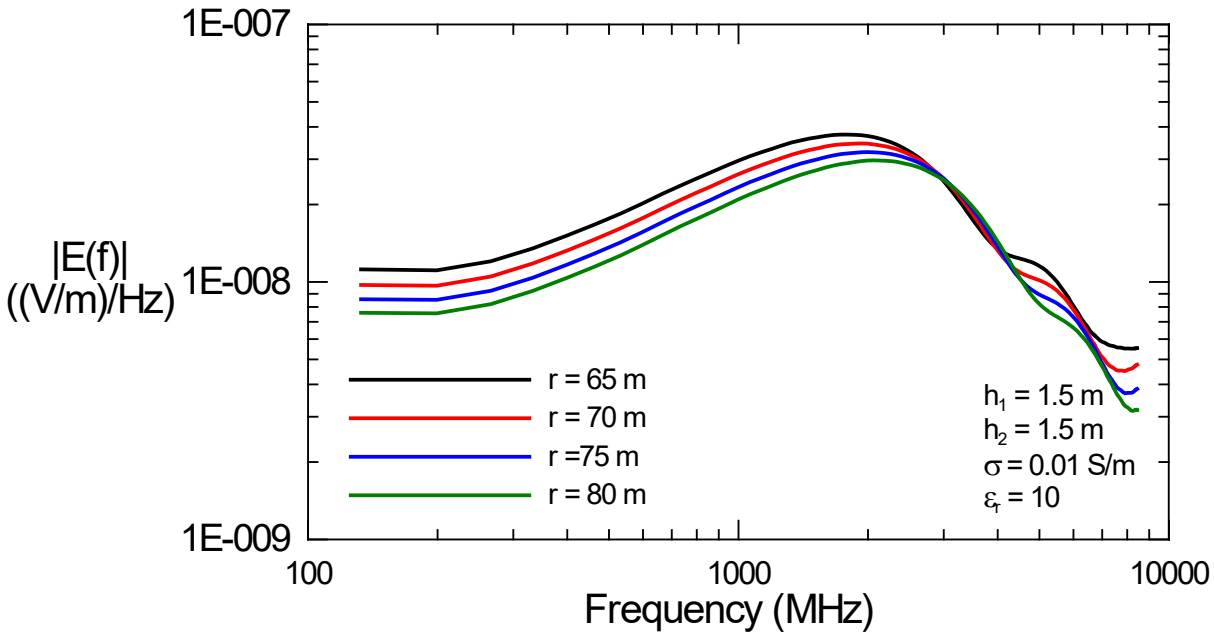

h. Spectral response for d = 65 to 80 m

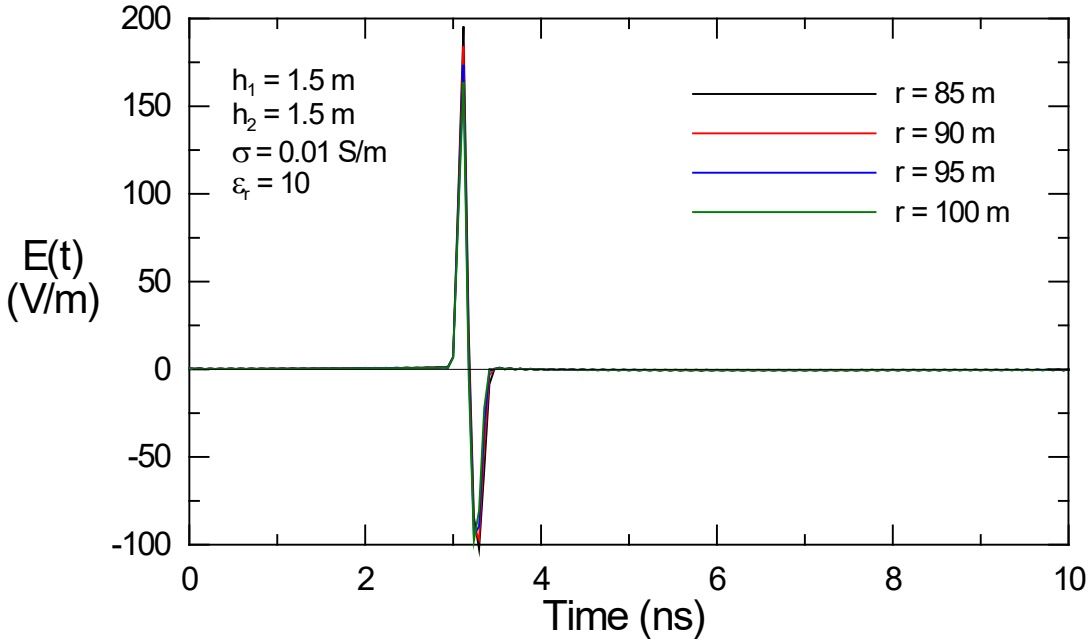

i. Transient response for d = 85 to 100 m

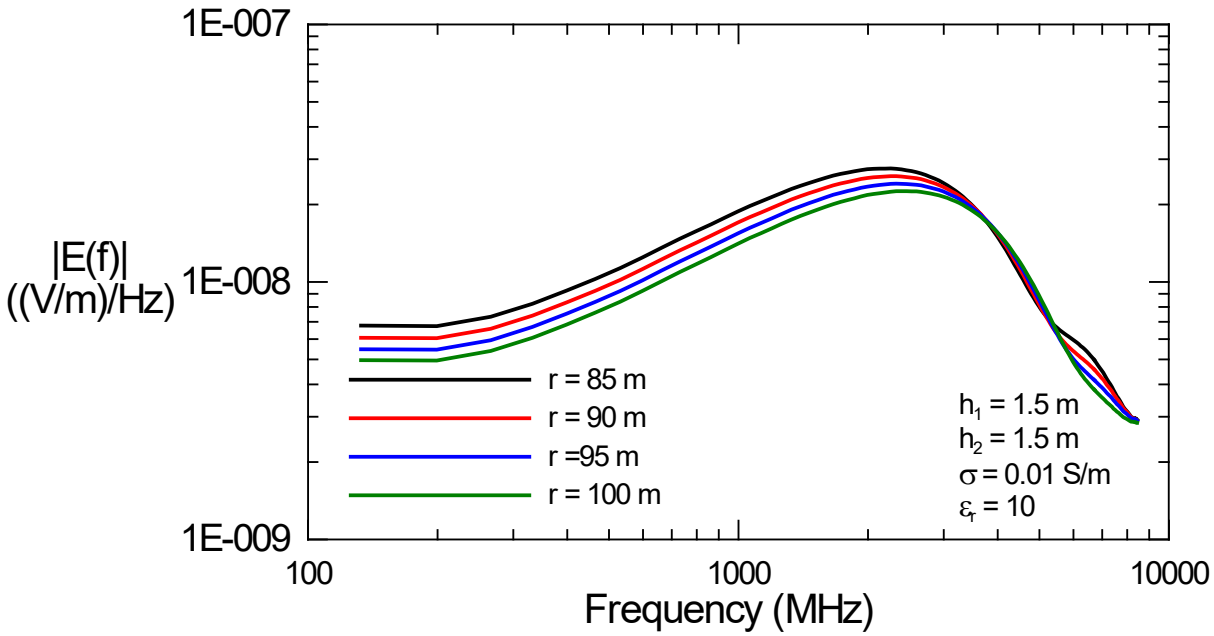

j. Spectral response for d = 85 to 190 m

Figure 24. Plots of the transient (top) and spectral (bottom) responses of the IRA fields for a source and observation height of 1.5 m over a lossy earth of $\sigma = 0.01$ S/m and $\varepsilon_r = 10$, for various distances of the observation location.

In comparing the calculated results presented in Figure 24 with the measured results of Figure 19, we note that there are differences between the estimated and measured fields. For example, there is an approximate factor of 2 discrepancy in the peak electric field at distances > 10 m.

There are several possible reasons for this, which include the following:

- The computed fields are based on the analytical expression for the pulser voltage, which is plotted in Figure 8. For the real pulser, the actual excitation voltage waveform may be considerably different, and this would impact strongly the amplitude of the radiated field, since the radiation is proportional to the derivative of the excitation voltage.

- Even if the excitation of Figure 8 were to be applied to the feed structure of the IRA, there can be a considerable difference in the excitation E-field in the aperture of the IRA, due to parasitic element effects in the transmission lines connecting the pulser source to the antenna.

- The feeder arms of the IRA are connected to the parabolic dish structure through termination resistances designed to "match" the dish to the characteristic impedance of the feed structure -- 400 Ω. If this matching is not done perfectly, there may be a discrepancy between the measured and calculated fields.

- The computational model assumes a cylindrical wire feed structure to compute the TEM mode distribution over the IRA aperture. In the physical model, these feeds are comprised of metal strips.

Notwithstanding these difficulties, the computational model for the IRA fields in the vicinity of the lossy earth is useful in assisting in the understanding of the radiation phenomenon from this antenna.

5. Summary and Conclusions

This note has summarized the transient and CW testing of a Swiss Civil Defense prototype facility, which took place in October 2000. For the transient excitation of the facility, which was located at the Spiez NEMP Laboratory, the Swiss impulse-radiating antenna (IRA) was used, and transient EM fields and currents within the facility were recorded. For the CW measurements, the same IRA antenna was used, but it was driven by an RF power amplifier, which in turn, was controlled by a network analyzer.

To summarize the transient responses, the pulsed voltage source feeding the IRA had a peak amplitude of 2.8 kV, a rise time of 100 ps, and an exponential decay time of about 2 ns. This source and antenna provided an impulse-like excitation to the facility, which at a distance of 6 m from the antenna had a peak value of about 1.1 kV/m.

For this source, the following transient field and current measurements were observed within the facility.

- Peak internal E-fields in stair well – 200 V/m (main door open); 60 V/m (main door closed)
- Peak internal E-fields in chamber next to stair well bottom –100 V/m (main door open)
- Peak E-fields in facility interior with propagation through overburden – 160 V/m
- Current on telecom lines –10-20 ma, depending on transmitter location
- Peak current on power ground/neutral phase conductor – 6.0 ma for IRA illuminating switching panel; 0.6 ma for IRA illuminating facility through overburden

These measurements shed light on some interesting effects pertaining to shielded and buried facilities. First, we have noted that there can be measurable EM fields induced inside a facility by shining the source through the earth overburden and buried facility roof. Of course, these fields are significantly attenuated by the earth, but nevertheless, they are present. If the IRA source pulser were increased by an order of magnitude, say to 28 kV, the resulting internal field would be on the order of 1 – 2 kV/m, which has the potential to do damage or cause upset to internal equipment. Such an enhanced pulser is certainly feasible given today's current pulser technology.

A second important issue is that well-defined current pulses were detected on the communication lines within the facility. Furthermore, larger responses were noted when the antenna was positioned to illuminate the region away from the main door, which contained the telephone connection box. We believe that the EM source was able to couple low-frequency energy into the buried telephone cables entering the facility, and this energy was subsequently injected into the facility. With the larger pulser mentioned above currents on the order of 0.1 to 0.2 A on such lines would be expected. Such excitation modes for internal equipment remain a concern for buried facilities, and internal system susceptibilities must be compared with these estimated response levels to make a definite statement about the overall system response to this external EM excitation.

The power system, however, is less of a concern. On this system a significantly lower response was noted (0.6 – 6 mA for the 2.8 kV pulser). Generally, the power system is much more robust that is the communication system, due to its larger operating voltage of 220 V, and the fact that there are many transient events daily on the power mains due to the normal operation of the system. Moreover, most electrical equipment have filters or other capacitive inputs on the incoming power lines to remove the normal line transients, and they should be able to withstand these HPEM-induced surges. Consequently, we believe that the power system will not be a significant issue for Civil Defense facilities.

Regarding the CW measurements for this facility, the test was successful in showing the equivalence between the CW transfer functions and those obtained using the Fourier transformed transient data. For these measurements, the actual raw measurements seem robust, and are well above the noise floor of the equipment. The IRA antenna worked very well in the CW mode, and this test concept should be considered again for future testing.

Finally, the seemingly anomalous behavior of the Swiss IRA has been studied and understood. The issue is that when the antenna is located over the earth, at certain distances there will be an earth-reflected E-field component that produces a more complex waveform illuminating the facility. This effect has been analyzed and modeled and has been discussed in this note.

6. References

1. F.M. Tesche and D.V. Giri, "High-power Electromagnetic (HPEM) Testing of Swiss Civil Defense Facilities, Volume IV –Spiez Facility Test Data", report for contract 4500300423 from the Swiss Defense Procurement Agency, Department of Defense, Civil Protection and Sports, September-November 2000. (Available from one of the authors DVG by e-mailing to: Giri@DVGiori.com)

2. F.M. Tesche, D.V. Giri, P.F. Bertholet, A. Jaquier, and A.W. Kaelin, "Measurements of High-Power Electromagnetic Field Interaction with a Buried Facility", paper presented at International Conference on Electromagnetics in Advanced Applications (ICEAA), Torino, Italy, September 10-15, 2001.

3. F.M. Tesche and D.V. Giri, "High-power Electromagnetic (HPEM) Testing of Swiss Civil Defense Facilities, Vols. I – III", report for contract 4500300423 from the Swiss Defense Procurement Agency, Department of Defense, Civil Protection and Sports, September-November 2000. (Available from one of the authors DVG by e-mailing to: Giri@DVGiori.com)

4. HYPS Pulse Source, S/N 5046, Grant Applied Physics, San Francisco, CA.

5. F. M. Tesche, et. al., **EMC Analysis Methods and Computational Models**, John Wiley and Sons, New York, 1997.

6. E. G. Farr, and C. A. Frost "Development of a Reflector IRA and a Solid Dielectric Lens IRA, Part I: Design, Predictions, and Construction, *Sensor and Simulation Notes*, Note SSN 396, April 1996.

Appendix I

Measurements of High-Power Electromagnetic Field Interaction with a Buried Facility

PowerPoint Presentation at **I**nternational **C**onference on
Electromagnetics in **A**dvanced **A**pplications (ICEAA)
Torino, Italy
September 10-15, 2001.

We have included this presentation because it contains additional measurement data not in the main body of this Note.

Drs. Tesche and Giri were at this conference on that fateful day of "Nine Eleven"

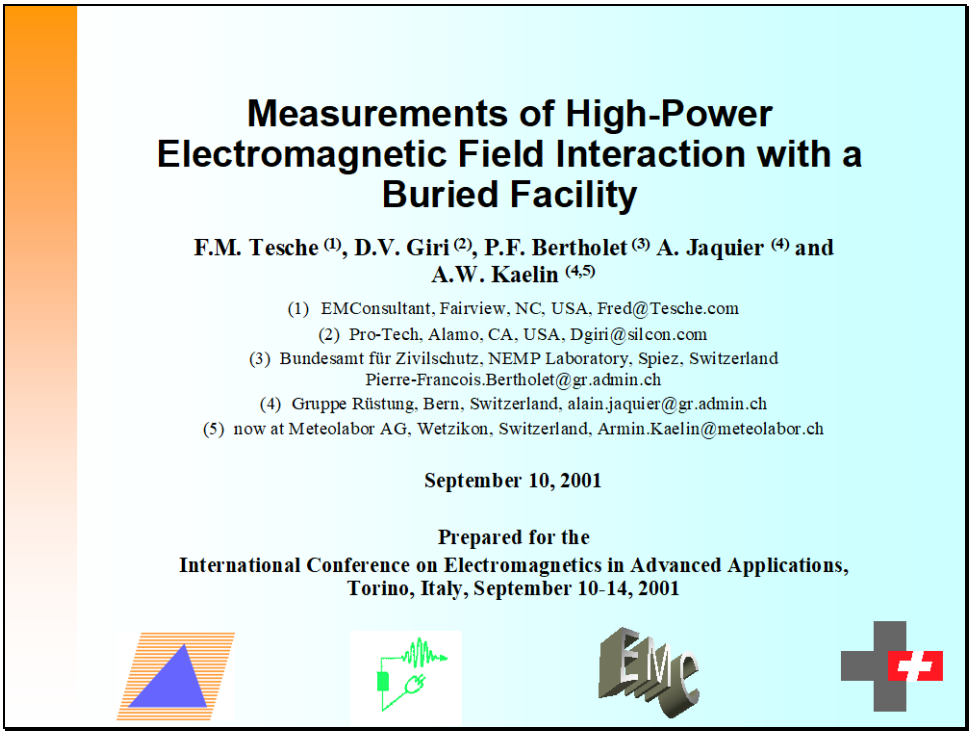

Measurements of High-Power Electromagnetic Field Interaction with a Buried Facility

F.M. Tesche [1], D.V. Giri [2], P.F. Bertholet [3] A. Jaquier [4] and A.W. Kaelin [4,5]

(1) EMConsultant, Fairview, NC, USA, Fred@Tesche.com
(2) Pro-Tech, Alamo, CA, USA, Dgiri@silcon.com
(3) Bundesamt für Zivilschutz, NEMP Laboratory, Spiez, Switzerland
Pierre-Francois.Bertholet@gr.admin.ch
(4) Gruppe Rüstung, Bern, Switzerland, alain.jaquier@gr.admin.ch
(5) now at Meteolabor AG, Wetzikon, Switzerland, Armin.Kaelin@meteolabor.ch

September 10, 2001

Prepared for the
International Conference on Electromagnetics in Advanced Applications,
Torino, Italy, September 10-14, 2001

Outline of Presentation

- **Overview**
- **Facility Description**
- **Measurement Configurations and Equipment**
- **Transient Responses**
- **CW Responses**
- **Summary**

Overview of Measurement Program

- In October 2000 a measurement program for HPEM interaction with Swiss Civil Defense (CD) facilities was conducted Switzerland
  - The rationale was to better understand high frequency or fast-pulse interaction with previously EMP-hardened facilities
  - The test object was a prototype facility located at the NEMP Laboratory in Spiez, Switzerland.
- Goals were to
  - Determine if there are significant EM field penetrations into buried facilities for frequencies up to several GHz
  - Develop and explore facility test techniques using the IRA
  - Compare system transfer functions developed from transient data with frequency domain measurements

Overview of Measurement Program (con't)

- Depending on further analysis of the measured data, full-scale testing on large Civil Defense facilities may be conducted in 2002.
  - To assess the possible effects of HPEM environments on these installations

Outline of Presentation

- Overview
- **Facility Description**
- Measurement Configurations and Equipment
- Transient Responses
- CW Responses
- Summary

Facility Description

- The facility tested was a small, buried concrete building
  - Originally constructed in a manner similar to real CD facilities
    - But without EMP protection installed
  - Main use of building was to test equipment installation procedures
    - Such as overpressure protection, air filters, etc.
- Facility features include
  - Rebar-reinforced concrete construction and buried in the earth,
  - Small above-ground concrete structure provides protection for the stairway leading from the surface to the working area below,
  - Two personnel escape hatches in the back part of the building
  - Blast-hardened doors leading to tunnels to the surface, and
  - Blast doors in each compartment inside the facility.

Facility Description (con't)

Illustration of exterior entrance on top of facility

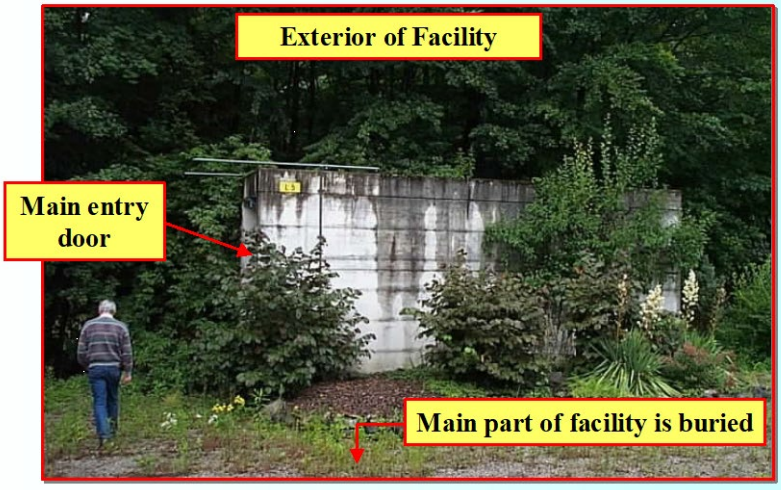

Facility Description (con't)

Illustration of floor plan of facility

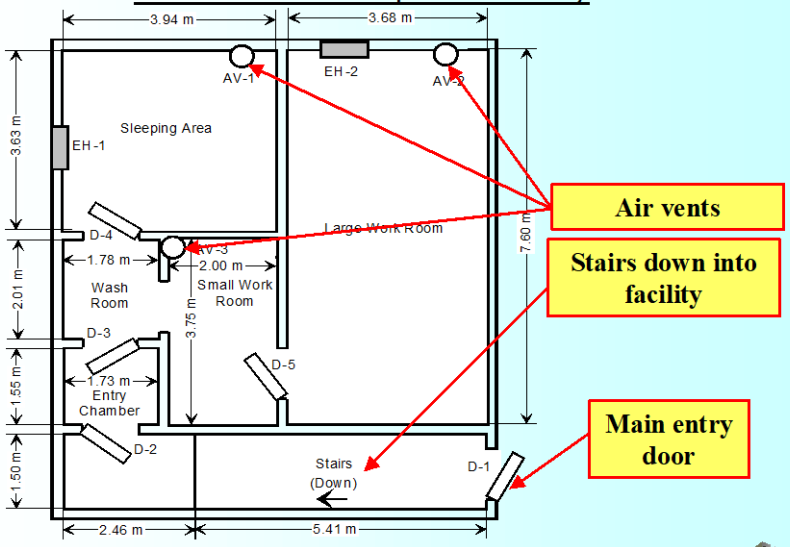

Outline of Presentation

- Overview
- Facility Description
- **Measurement Configurations and Equipment**
- Transient Responses
- CW Responses
- Summary

Measurement Concept

- Use the Swiss impulse radiating antenna (IRA) to perform both transient and CW transfer function measurements into the facility
- Four different measurement groups (MG) were defined

MG	Title
1	Noise Measurements
2	IRA Transient Characterization
3	IRA Frequency Domain Characterization
4	Facility Measurements

Equipment Configurations

Equipment configuration for facility measurements (MG-4)

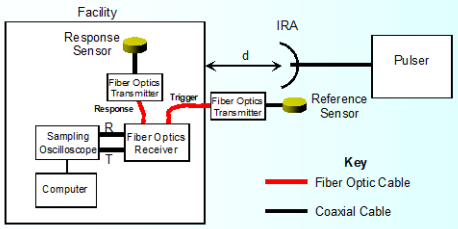

Transient Measurements

Frequency Domain

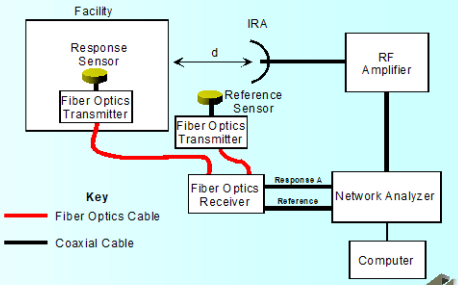

Description of the Swiss IRA

- The antenna is a standard parabolic IRA design
  - D = Reflector antenna diameter =1.8m
  - F = Focal length of the reflector = 0.48m
  - F/D = Focal length / Diameter = 0.267
- Transient pulser output:
  - Peak output voltage = 2.8 kV
  - Rise time 100 ps,
  - Full width to half-max = 2 ns.

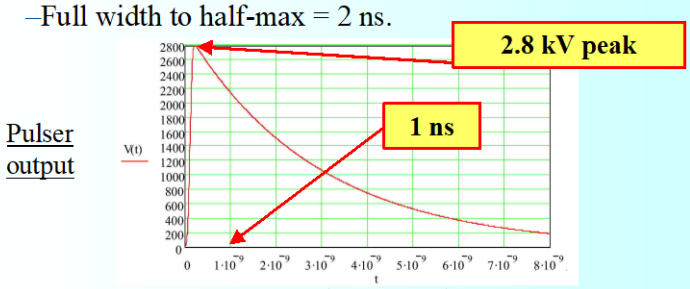

Description of the Swiss IRA (con't.)

Calculated near and far transient field on boresight at various distances from the Swiss IRA

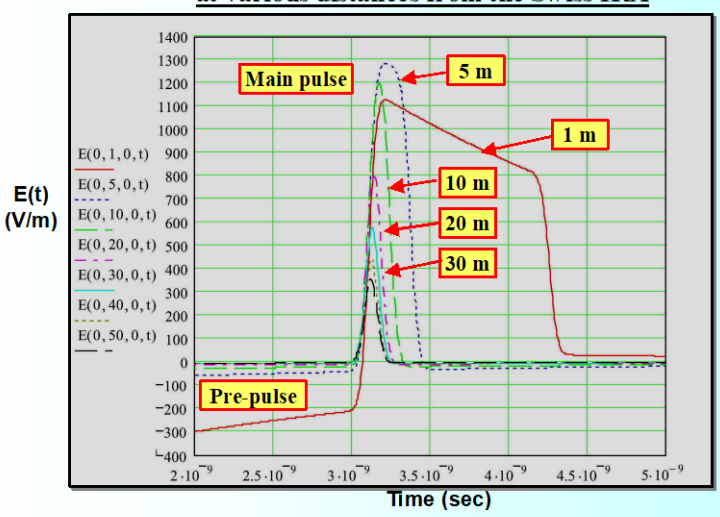

Description of the Swiss IRA (con't.)

Calculated E- field spectral magnitude on boresight at various distances from the Swiss IRA

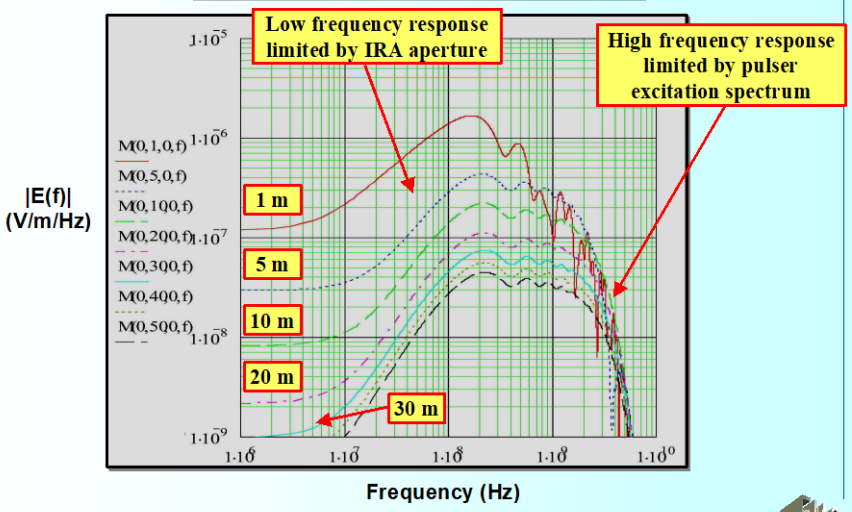

Description of the Swiss IRA (con't.)

Measured IRA E-field at a distance of 6 m from the Swiss IRA

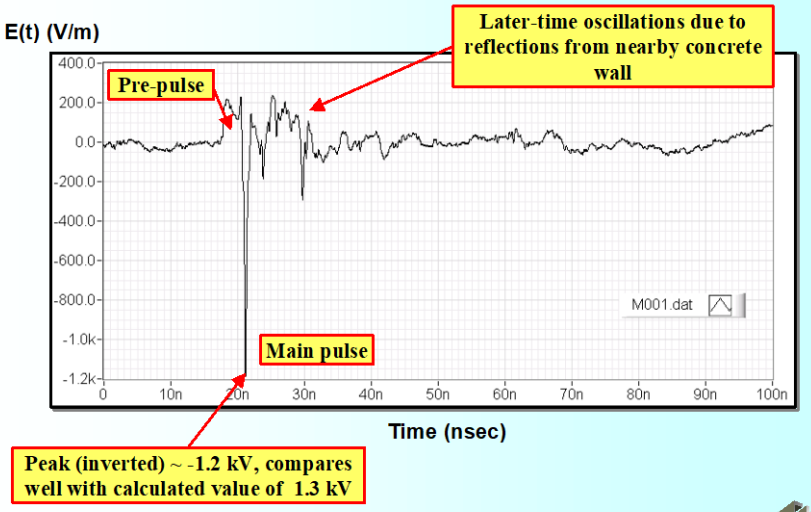

Source and Measurement Locations

Facility plan showing excitation and measurement locations

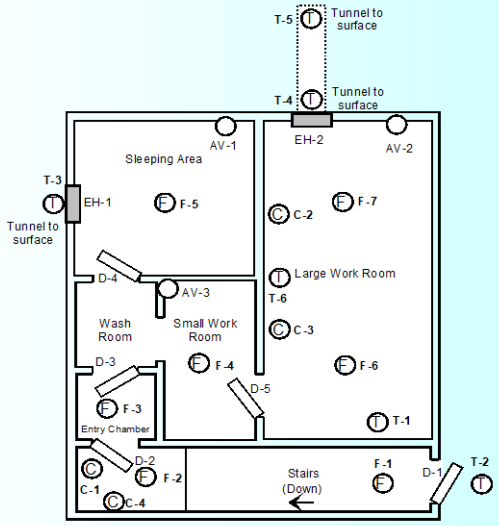

Outline of Presentation

- Overview
- Facility Description
- Measurement Configurations and Equipment
- **Transient Responses**
  - **E-fields**
  - Currents
- CW Responses
- Summary

Examples of Measured Field Responses

Attenuation of E-field passing thru concrete wall at facility entrance

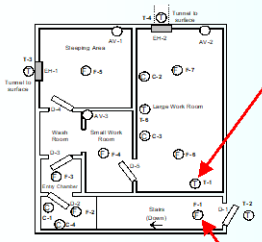

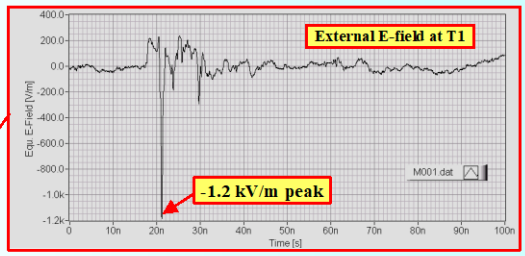

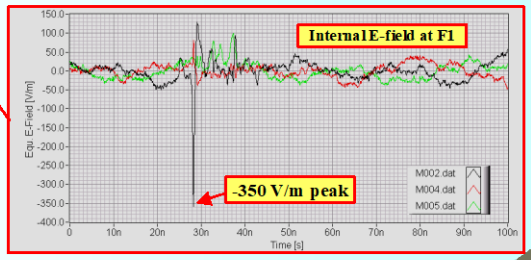

Concrete wall with rebar provides an attenuation of the peak E-field of ~ 10.7 dB.

Examples of Measured Field Responses

E-field in entryway passage, illuminated from T2

IRA source at T2 (2.85 m from front door)

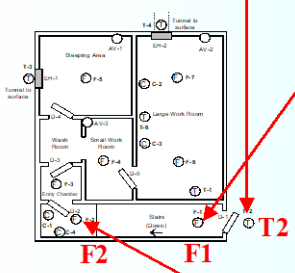

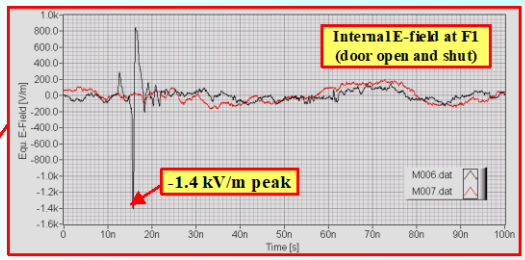

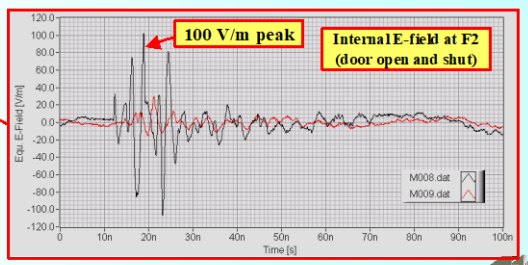

- E-field reduction from F1 to F2 is ~ 23 dB (1/r scaling gives only 17 dB)
- Significant ringing occurs in response at F2
- Field reduction due to shutting door is significant

Examples of Measured Field Responses

E-field in interior rooms, illuminated from T2

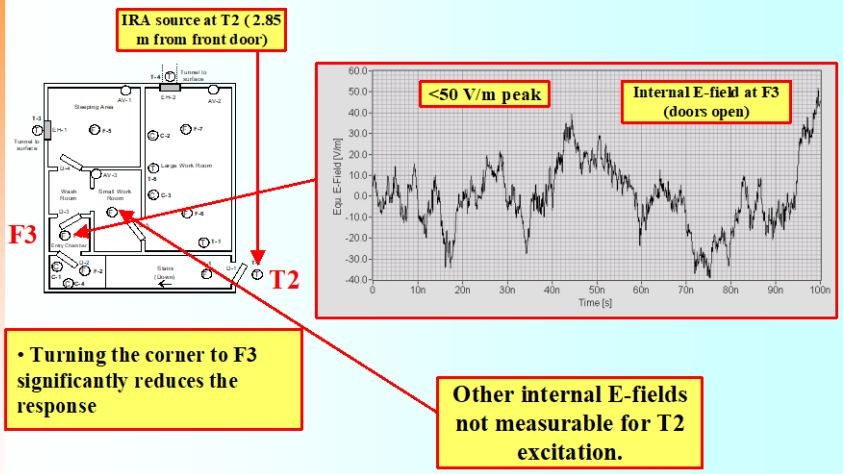

Examples of Measured Field Responses

E-field in interior rooms at F7, illuminated from T6

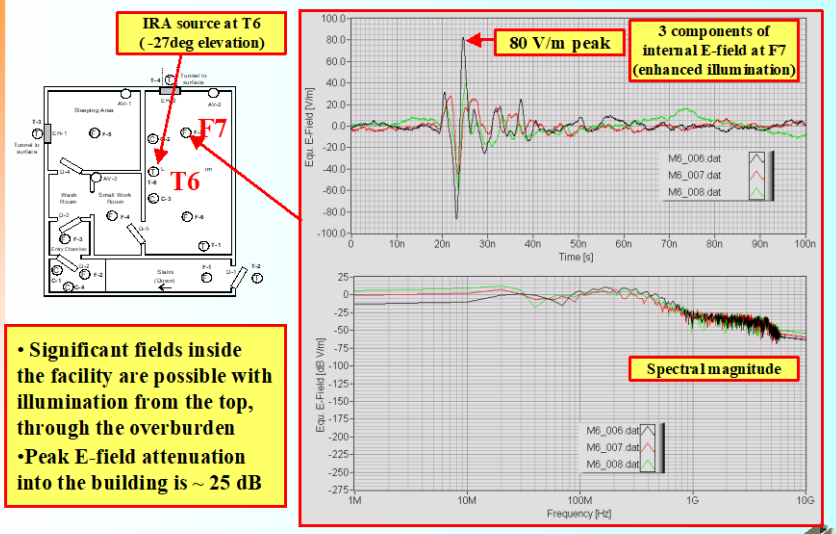

Examples of Measured Field Responses

E-field in interior rooms at F7, illuminated from T4

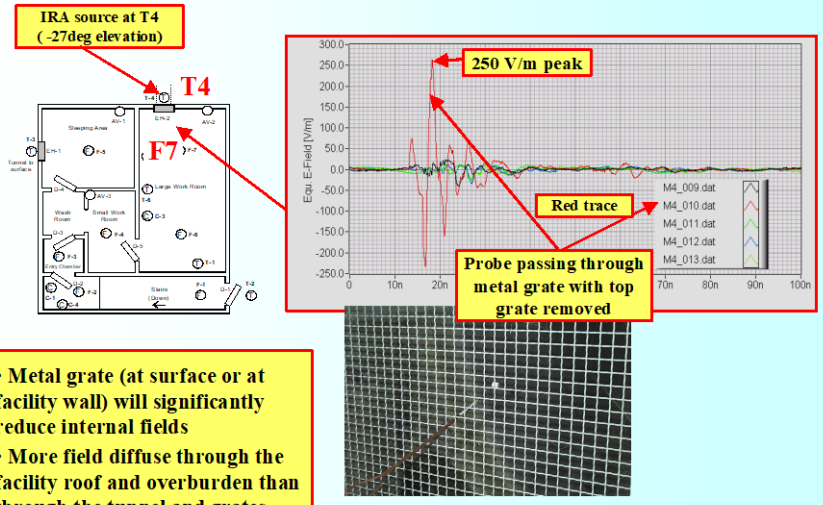

- Metal grate (at surface or at facility wall) will significantly reduce internal fields
- More field diffuse through the facility roof and overburden than through the tunnel and grates

Outline of Presentation

- Overview
- Facility Description
- Measurement Configurations and Equipment
- **Transient Responses**
  - E-fields
  - **Currents**
- CW Responses
- Summary

Examples of Measured Current Responses

Telephone line current at location C2, illuminated from T2

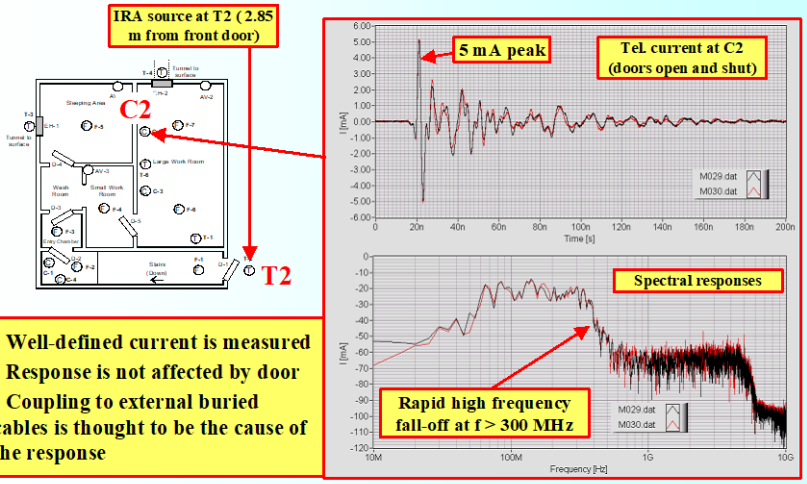

- Well-defined current is measured
- Response is not affected by door
- Coupling to external buried cables is thought to be the cause of the response

Examples of Measured Current Responses

Telephone line current at location C2, illuminated from T6

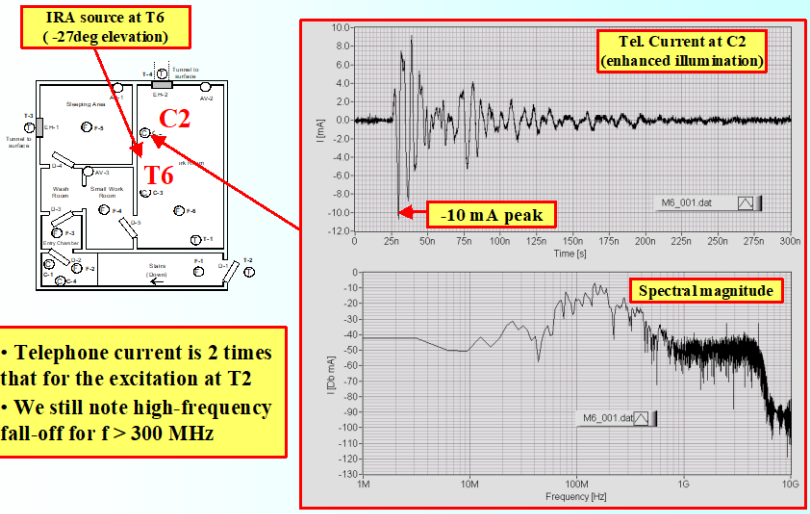

- Telephone current is 2 times that for the excitation at T2
- We still note high-frequency fall-off for f > 300 MHz

Examples of Measured Current Responses

Current on power system neutral (shorted to phase conductor) at location C3, illuminated from T2 in two directions

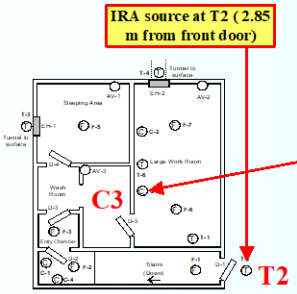

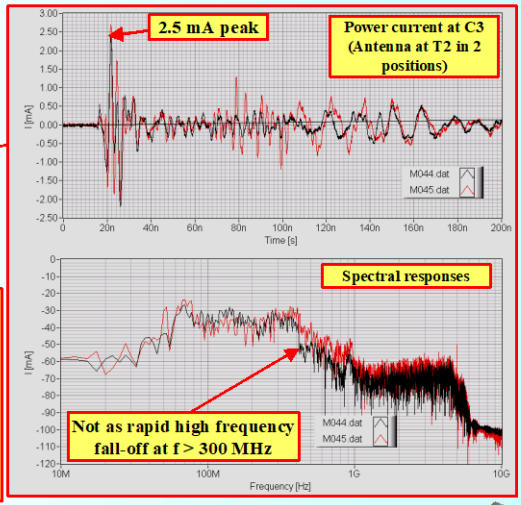

- As in the telephone measurement, well-defined waveforms are noted on the power system
- Antenna placement does not seem to be important for response
- Response is largest at low frequencies where the antenna beam is not very directional

Examples of Measured Current Responses

Current on power system neutral (shorted to phase conductor) at location C3, illuminated from T6

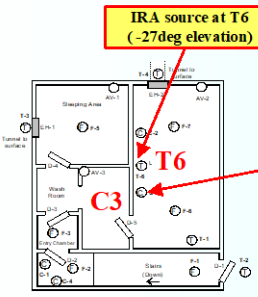

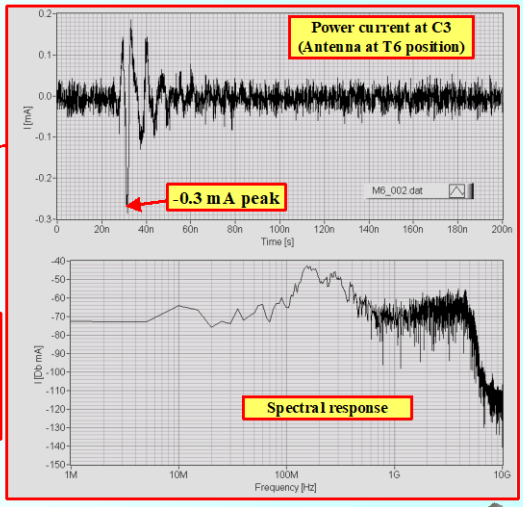

- Unlike the telephone measurement, the power system response here is less than for the T2 excitation (a factor of 10 smaller)

Outline of Presentation

- Overview
- Facility Description
- Measurement Configurations and Equipment
- Transient Responses
- **CW Responses**
- Summary

CW Transfer Functions

- CW transfer functions were also measured
  - Typically relating a measured H-field component to the applied IRA excitation voltage
- Example of H-field at F1 due to excitation at T2
  - Through concrete wall at entry stairs

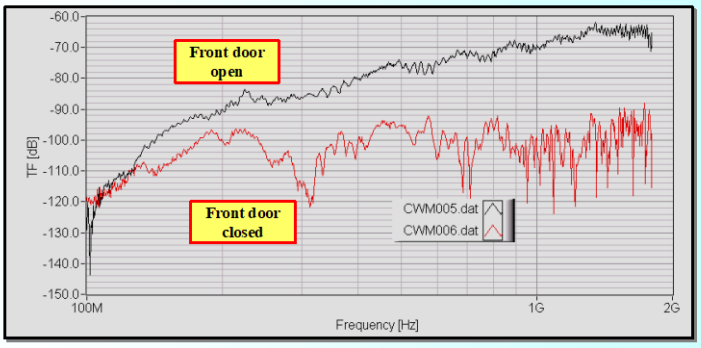

CW Transfer Functions (con't)

- H-field components at F2 (bottom of stairs) due to excitation at T2
  - –Door open and shut

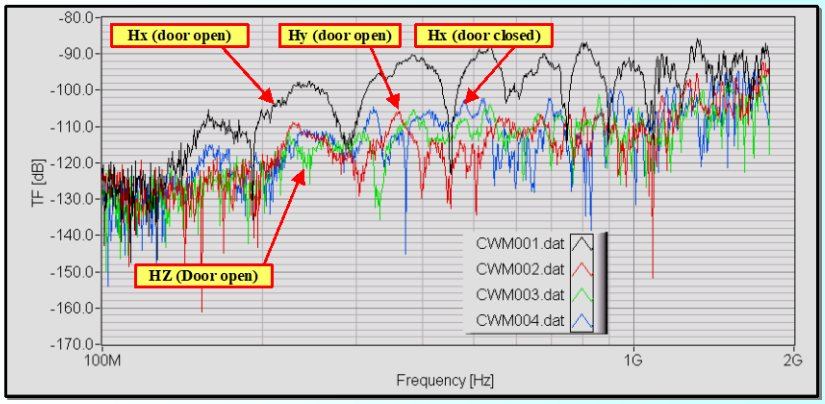

Outline of Presentation

- Overview
- Facility Description
- Measurement Configurations and Equipment
- Transient Responses
- CW Responses
- **Summary**

Summary

- Transient and CW measurements have been performed on a buried civil defense facility using an IRA source
- A transient 2.8 kV pulser produced an incident E-field environment of 1.2 kV/m at 6 meters
- This transient environment provided the following responses

Response and Location	Peak Response
Peak internal E-fields in stair well bottom	100 V/m (Main door open) 30 V/m (Main door closed)
Peak internal E-fields in chamber next to stair well bottom	50 V/m (Main door open)
Peak E-fields in facility interior with propagation through overburden	80 V/m
Current on telecom lines	5-10 ma, depending on transmitter location
Peak current on power ground/neutral phase conductor	3 ma for IRA illuminating switching panel 0.3 ma for IRA illuminating facility through overburden

Summary

- CW transfer function measurements have also been made
  - These data are still being analyzed
- Measurements provide a rough indication of HPEM responses in realistic buried facilities

Appendix II

Illustration of EM Field Penetration into a Lossy Earth

The behavior of planar EM fields, as they propagate from an overhead source into the earth, is well understood. As discussed in the EMC literature (Tesche, F.M., et. al., EMC Analysis Methods and Computational Models, John Wiley and Sons, New York, 1997), the behavior of the reflected and transmitted plane waves from the air-earth interface shown in Figure 1 can be described in terms of the Fresnel reflection and transmission coefficients, together with the electrical parameters of the earth.

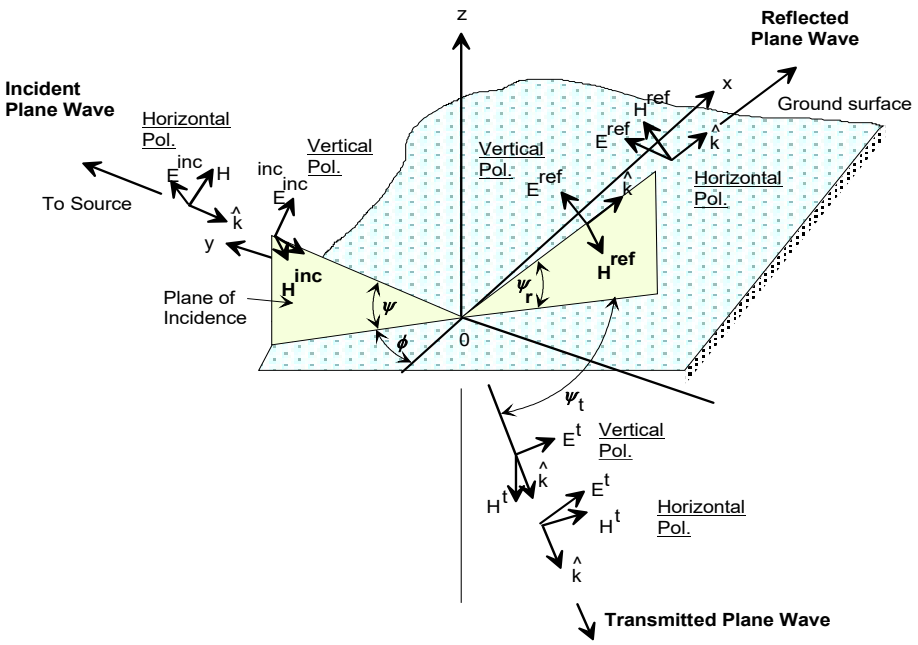

Figure 1. Reflected and transmitted waves at the air-earth interface

Using the relationships developed in [Tesche et al., cited above], the transmitted E-field has been computed as function of frequency and for various depths of the observation location. This has been done for an earth with a conductivity σ = 0.008 S/m and relative dielectric constant ε_r = 7.09, and the results are shown in Figure 2.

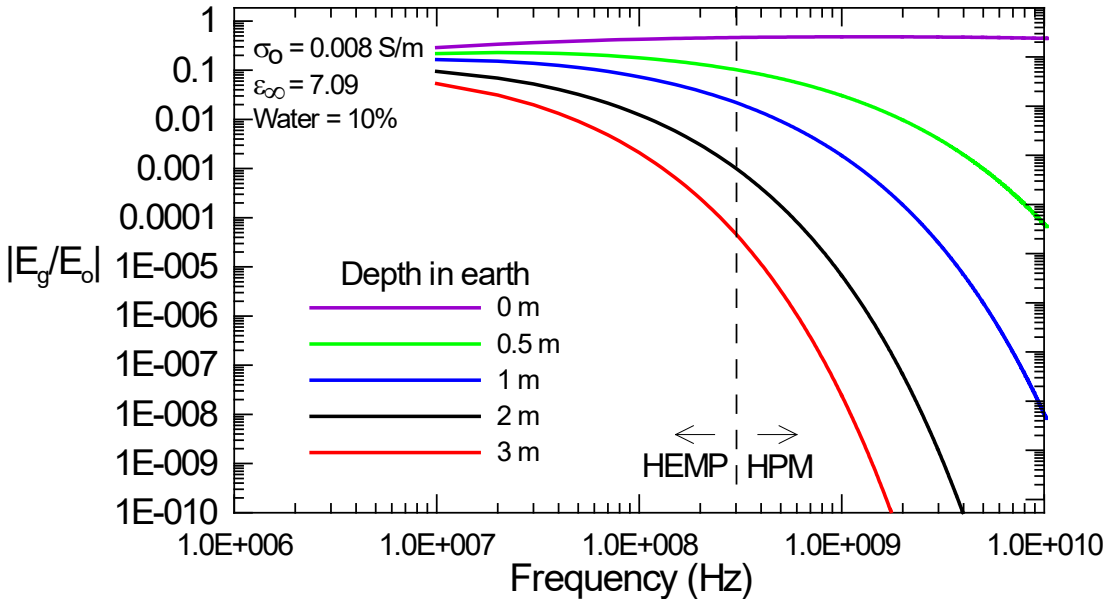

Figure 2. **Plot of the magnitude of the transmitted E-field into a lossy earth as a function of frequency, for different depths of the observation point.**